JOURNAL OF GLACIOLOGY

CAMBRIDGE UNIVERSITY PRESS

Characterising Ice Slabs in Firn Using Seismic Full Waveform Inversion

Journal:	*Journal of Glaciology*
Manuscript ID	JOG-22-0096
Manuscript Type:	Article
Date Submitted by the Author:	02-Sep-2022
Complete List of Authors:	Pearce, Emma; University of Leeds, School of Earth and Environment Booth, Adam; University of Leeds, School of Earth and Environment Rost, Sebastian ; University of Leeds School of Earth and Environment Sava, Paul; Colorado School of Mines, Department of Geophysics Konuk, Tugrul; Colorado School of Mines, Department of Geophysics Hubbard, Bryn; Aberystwyth University, Geography & Earth Sciences Brisbourne, Alex; British Antarctic Survey, IDP Jones, Ian; BrightSkies Geoscience
Keywords:	Glacier geophysics, Seismics, Seismology, Polar firn, Ice thickness measurements
Abstract:	The density structure of firn has implications for hydrological and climate modelling, and ice shelf stability. The structure of firn can be evaluated from depth models of seismic velocity, widely obtained with Herglotz-Wiechert Inversion (HWI), an approach that considers the slowness of refracted seismic arrivals. However, HWI is strictly appropriate only for steady-state firn profiles and the inversion accuracy can be compromised

	where firn contains ice layers. In these cases, Full Waveform Inversion (FWI) may yield more success than HWI. FWI extends HWI capabilities by considering the full seismic waveform and incorporates reflected arrivals. Using synthetic firn density profiles, assuming both steady- and non-steady-state accumulation, we show that FWI outperforms HWI for detecting ice slab boundaries (5-80 m thick, 5-80 m deep) and velocity anomalies within firn. FWI can detect slabs thicker than one wavelength (here, 20 m, assuming a maximum frequency of 60 Hz) but requires the starting velocity model to be accurate to ±2.5%. We recommend for field practice that the shallowest layers of velocity models are constrained with ground-truth data. Nonetheless, FWI shows advantages over established methods, and should be considered when the characterisation of firn ice slabs is the goal of the seismic survey.

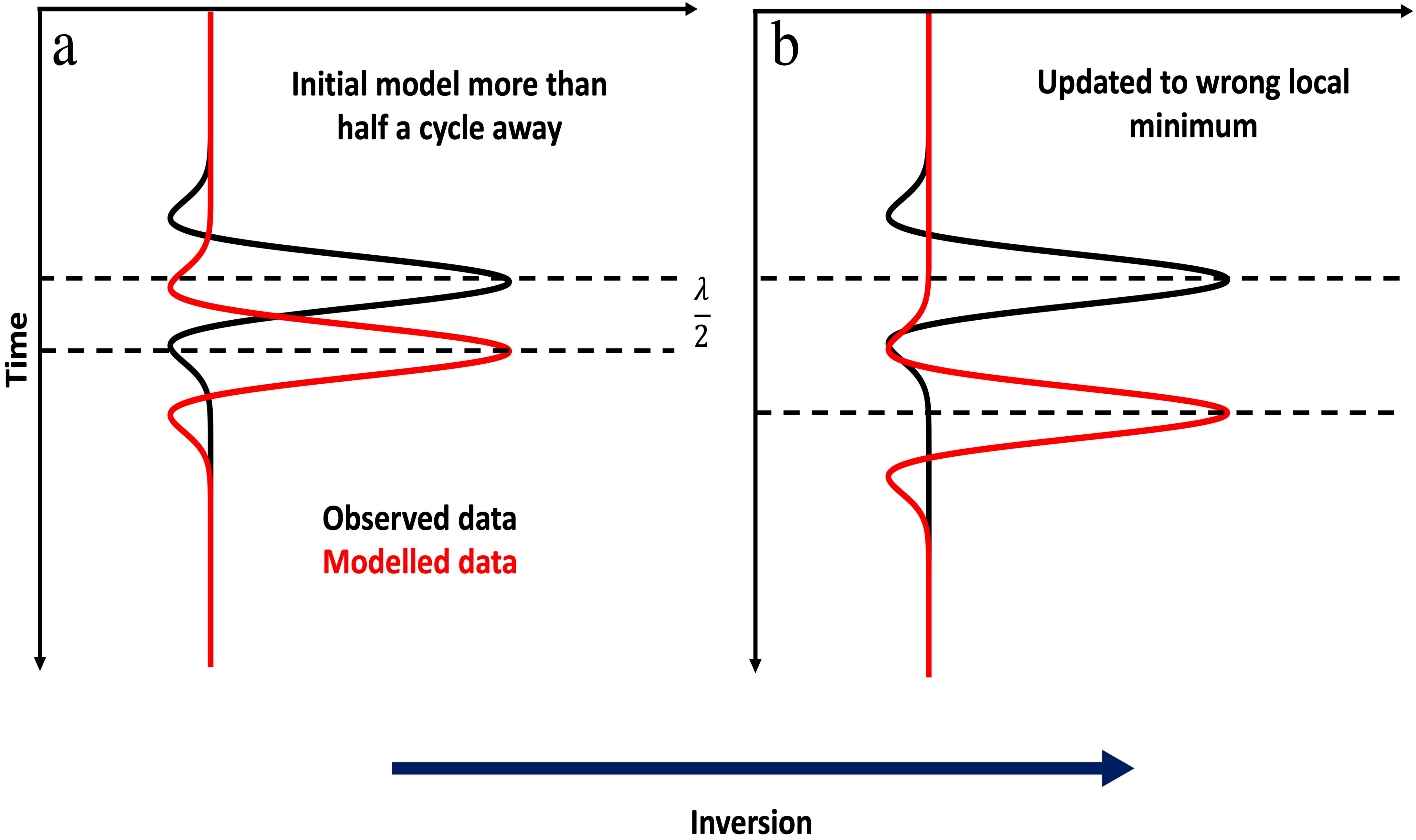
a
Initial model more than half a cycle away
$\frac{\lambda}{2}$
Time
Observed data
Modelled data
b
Updated to wrong local minimum
Inversion

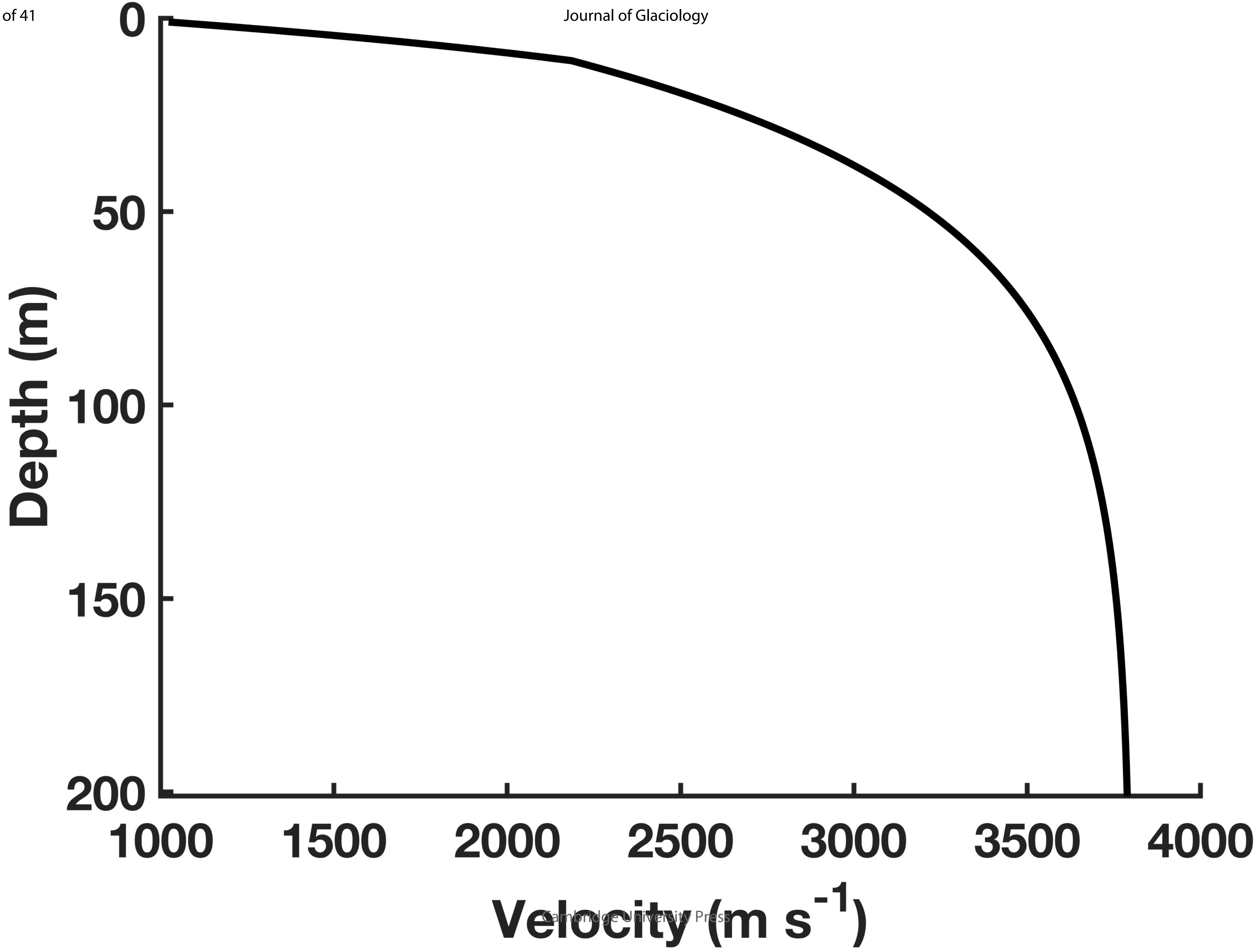
0
50
100
150
200
Depth (m)
1000
1500
2000
2500
3000
3500
4000
Velocity (m s^-1)

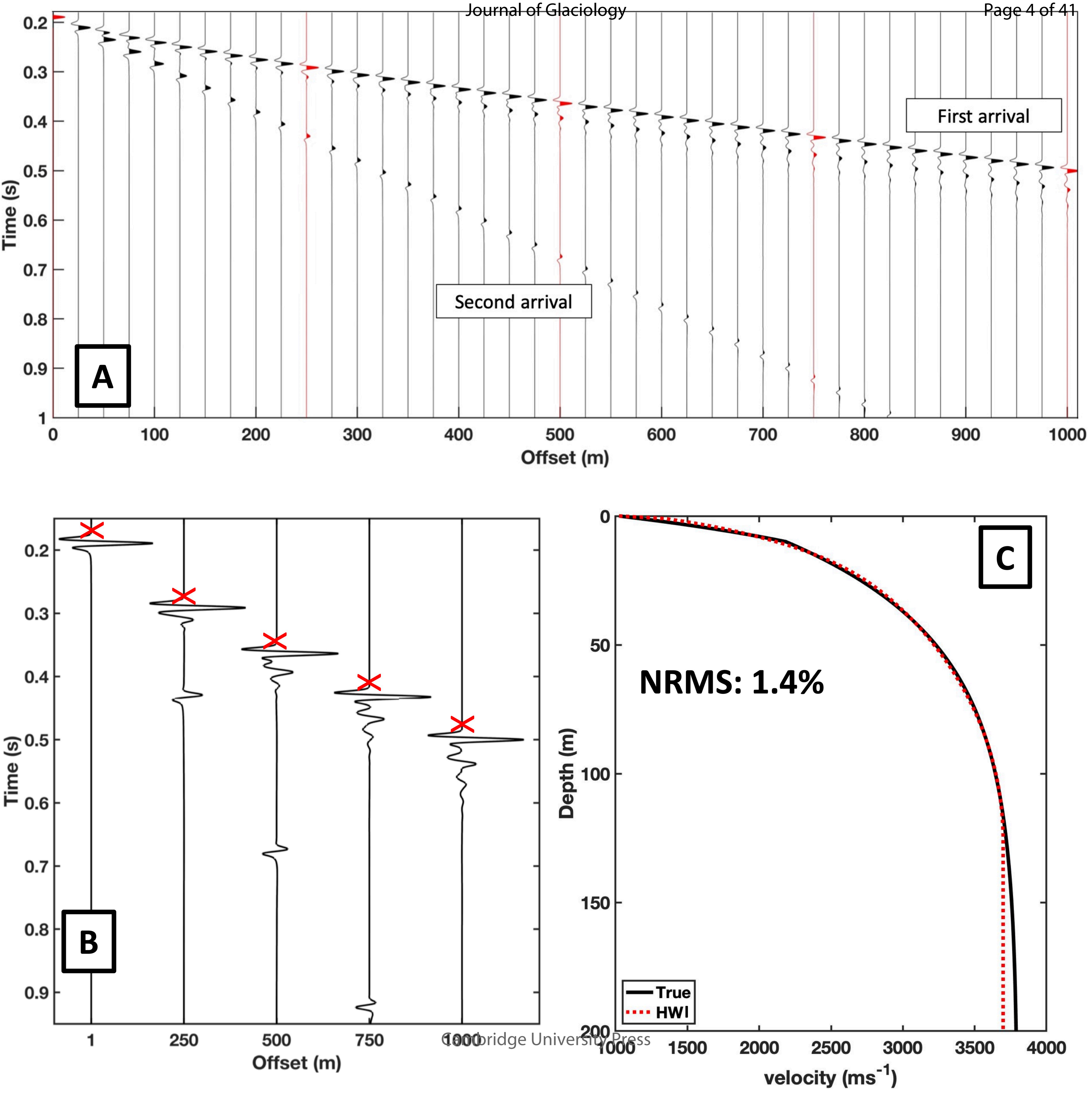

A
Time (s)
Offset (m)
First arrival
Second arrival
B
Time (s)
Offset (m)
C
NRMS: 1.4%
Depth (m)
velocity (ms^{-1})
True
HWI

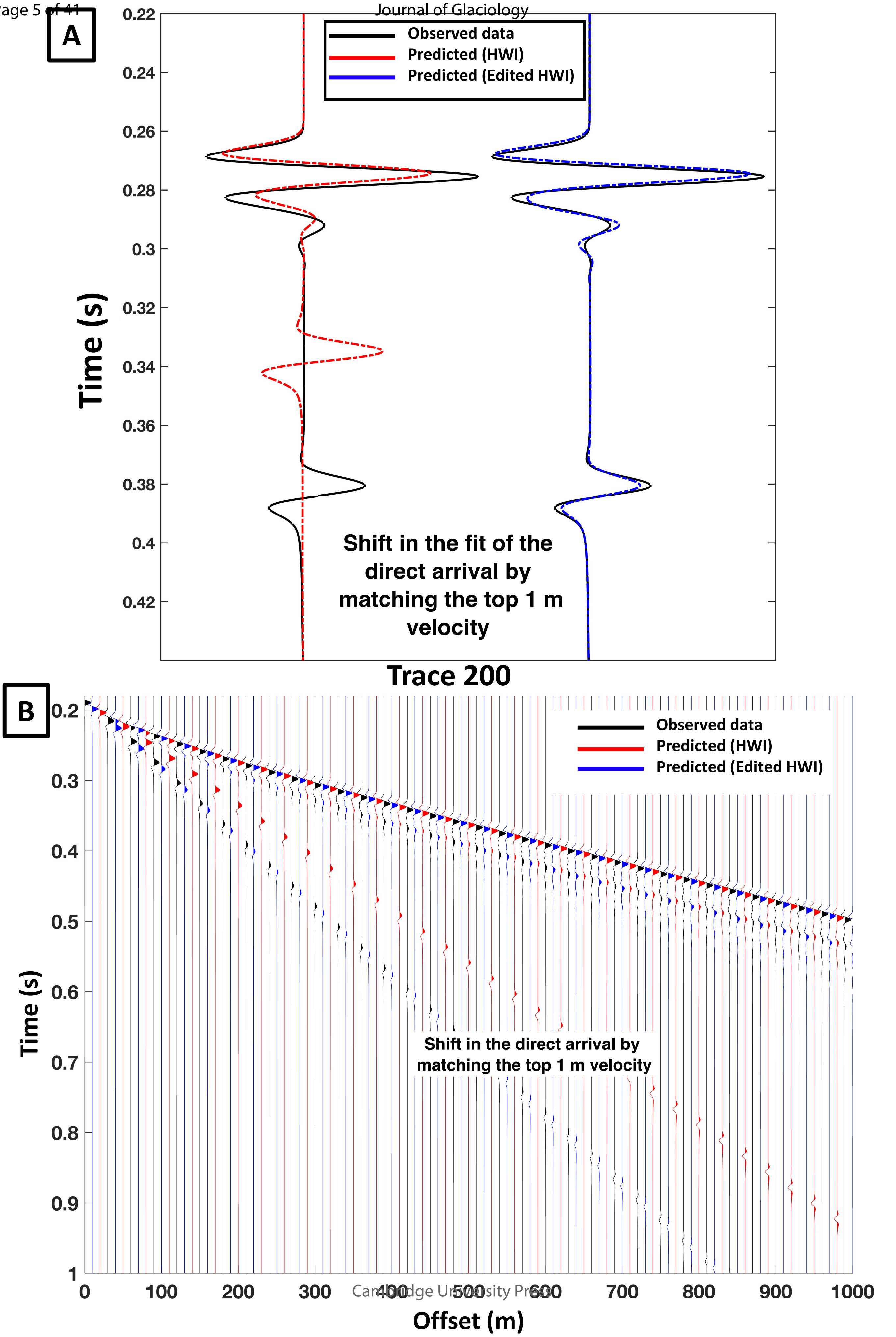
A
Observed data
Predicted (HWI)
Predicted (Edited HWI)
Time (s)
Shift in the fit of the direct arrival by matching the top 1 m velocity
Trace 200
B
Observed data
Predicted (HWI)
Predicted (Edited HWI)
Time (s)
Shift in the direct arrival by matching the top 1 m velocity
Offset (m)

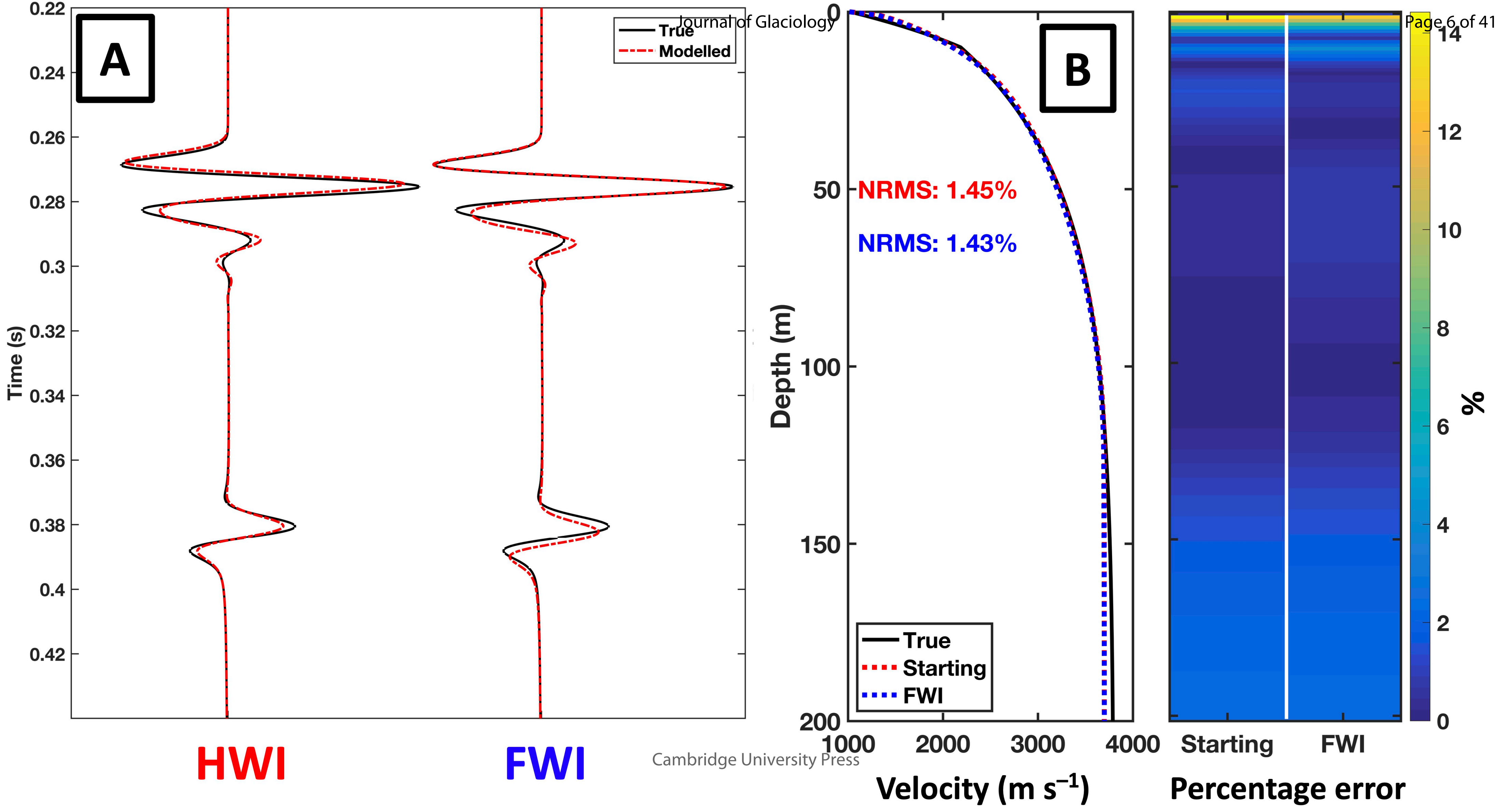
A
True
Modelled
Time (s)
0.22
0.24
0.26
0.28
0.3
0.32
0.34
0.36
0.38
0.4
0.42
HWI
FWI
B
NRMS: 1.45%
NRMS: 1.43%
Depth (m)
0
50
100
150
200
True
Starting
FWI
1000
2000
3000
4000
Velocity (m s−1)
Starting
FWI
Percentage error
%
0
2
4
6
8
10
12
14

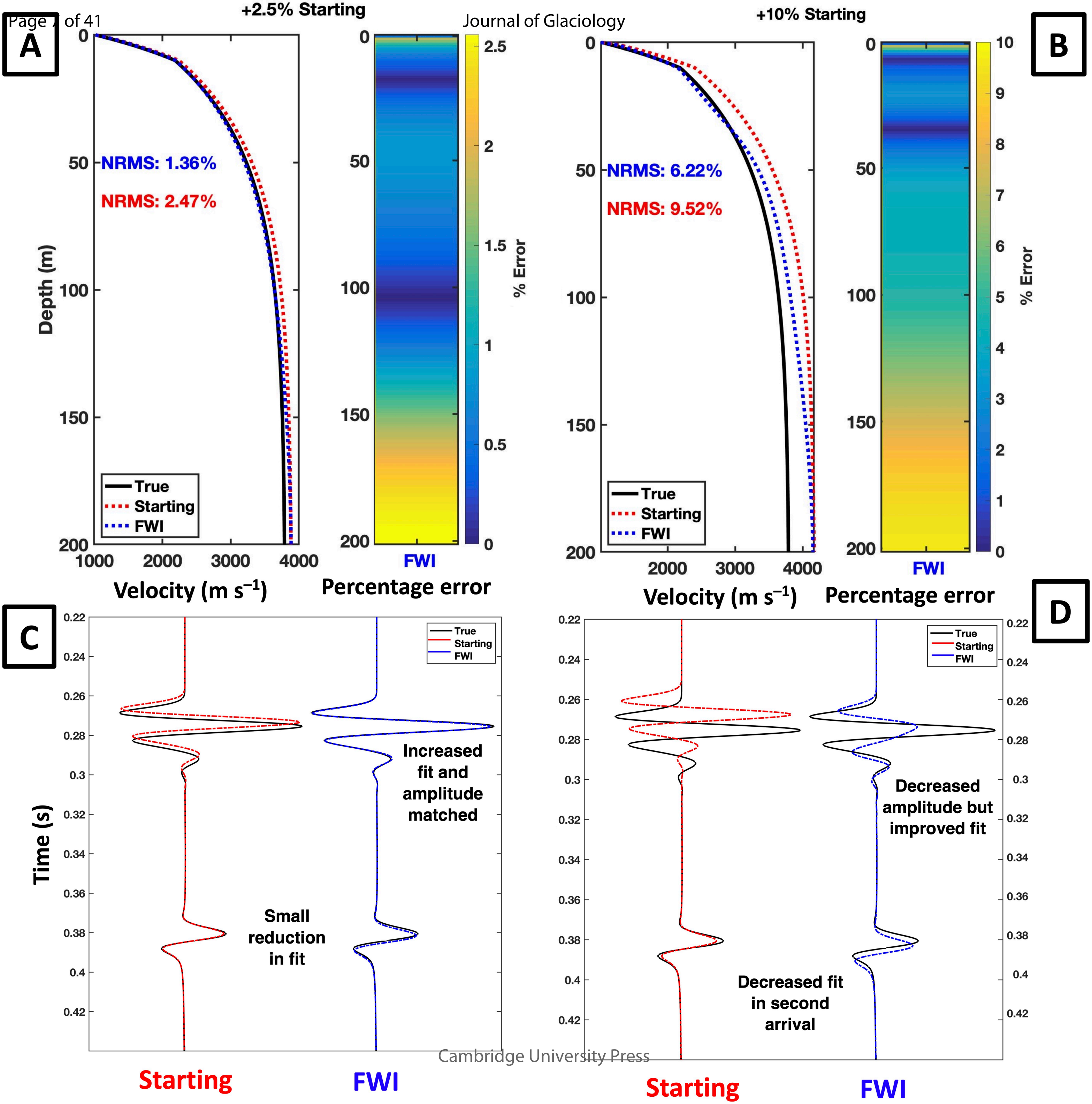

A
+2.5% Starting
Depth (m)
NRMS: 1.36%
NRMS: 2.47%
True
Starting
FWI
Velocity (m s−1)
% Error
FWI
Percentage error
B
+10% Starting
NRMS: 6.22%
NRMS: 9.52%
True
Starting
FWI
Velocity (m s−1)
% Error
FWI
Percentage error
C
Time (s)
Increased fit and amplitude matched
Small reduction in fit
Starting
FWI
D
Decreased amplitude but improved fit
Decreased fit in second arrival
Starting
FWI

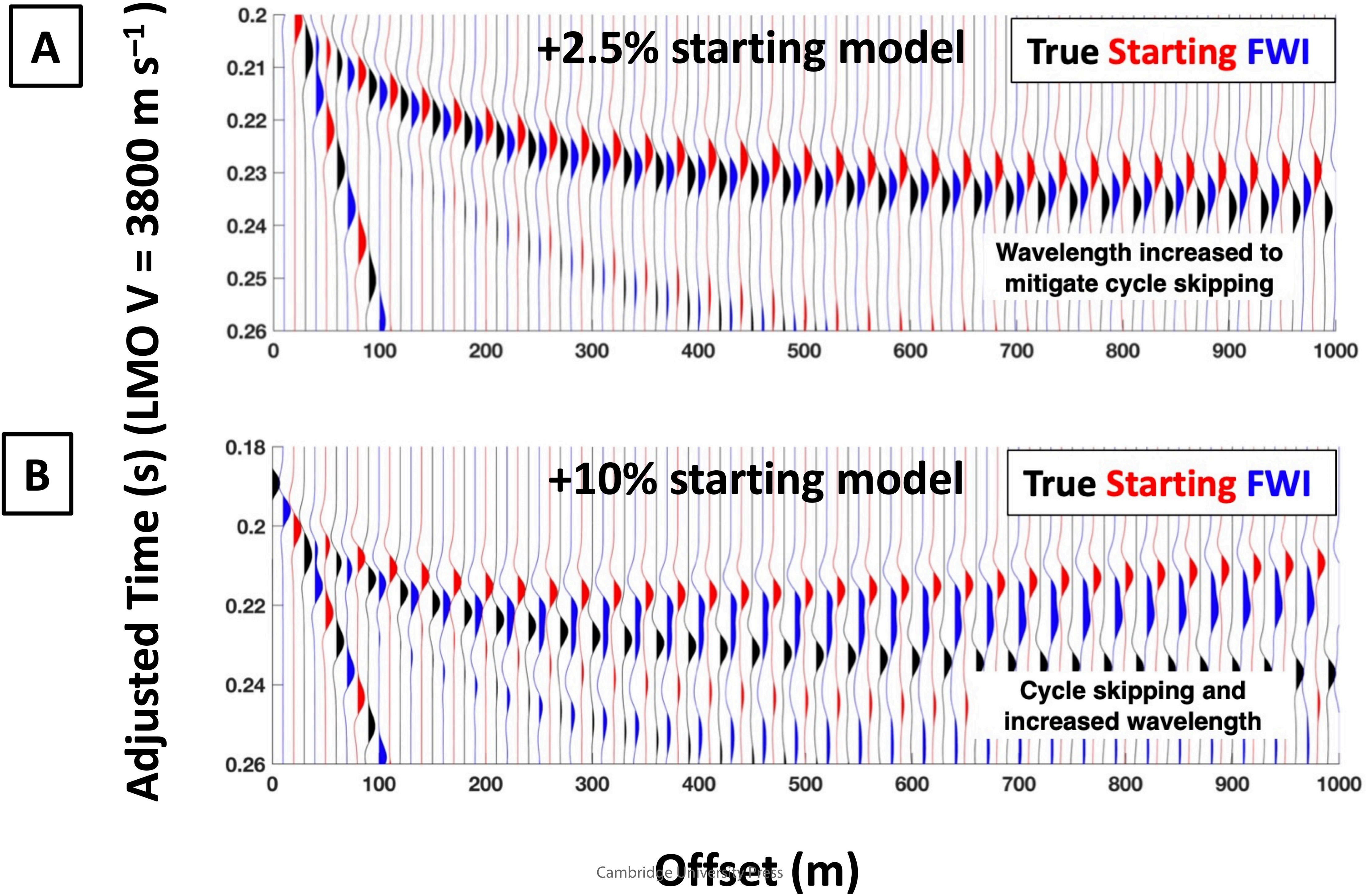
A
B
+2.5% starting model
True Starting FWI
Wavelength increased to mitigate cycle skipping
+10% starting model
True Starting FWI
Cycle skipping and increased wavelength
Adjusted Time (s) (LMO V = 3800 m s^{-1})
Offset (m)
0.2
0.21
0.22
0.23
0.24
0.25
0.26
0.18
0.2
0.22
0.24
0.26
0
100
200
300
400
500
600
700
800
900
1000

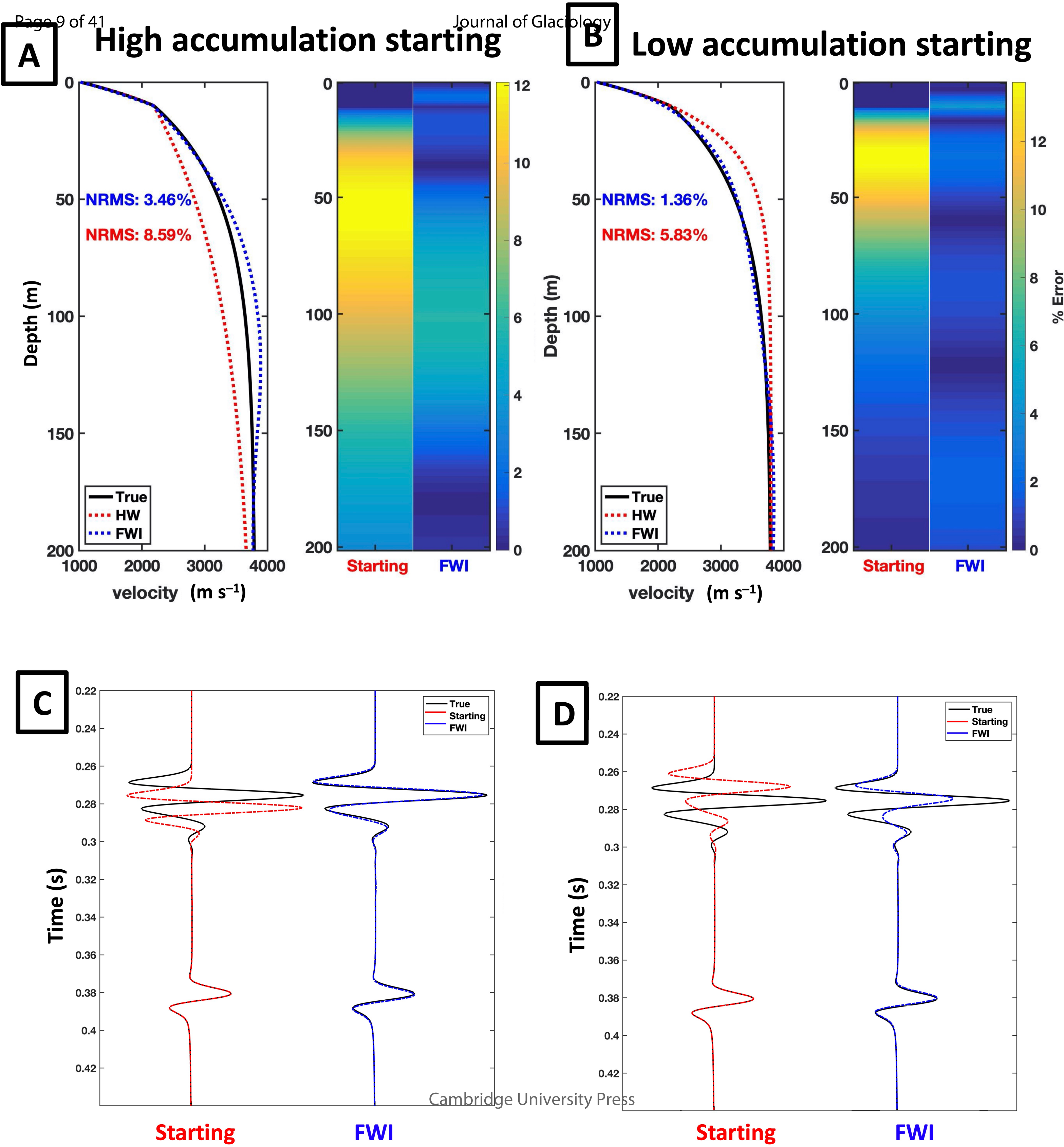

A
High accumulation starting
B
Low accumulation starting
NRMS: 3.46%
NRMS: 8.59%
NRMS: 1.36%
NRMS: 5.83%
Depth (m)
velocity (m s⁻¹)
True
HW
FWI
Starting
FWI
% Error
C
D
Time (s)
True
Starting
FWI

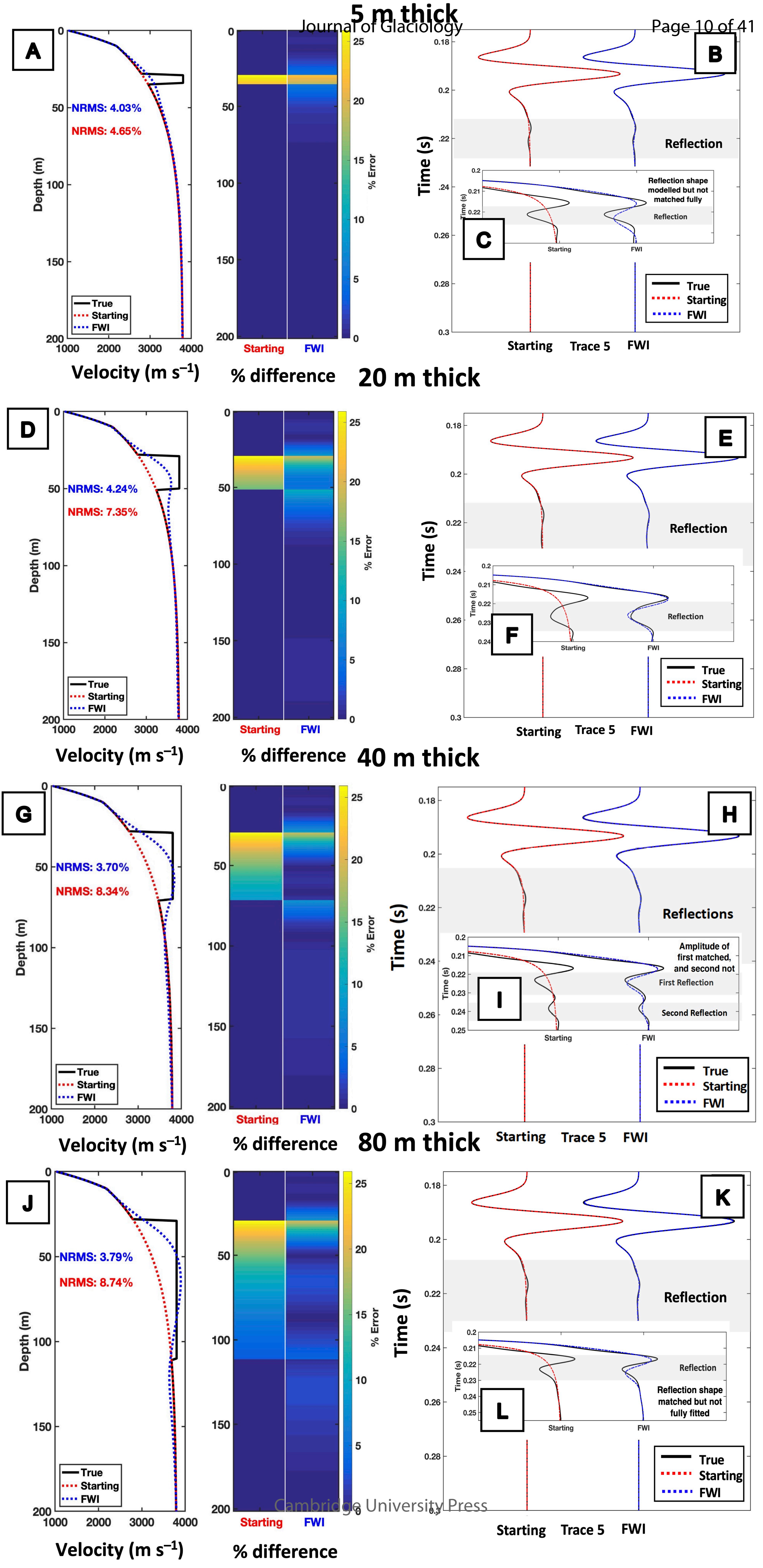
5 m thick
A
NRMS: 4.03%
NRMS: 4.65%
True
Starting
FWI
Depth (m)
Velocity (m s^{-1})
Starting
FWI
% Error
% difference
B
Reflection
Time (s)
Reflection shape modelled but not matched fully
Reflection
C
Starting
FWI
True
Starting
FWI
Starting
Trace 5
FWI
20 m thick
D
NRMS: 4.24%
NRMS: 7.35%
True
Starting
FWI
Depth (m)
Velocity (m s^{-1})
Starting
FWI
% Error
% difference
E
Reflection
Time (s)
Reflection
F
Starting
FWI
True
Starting
FWI
Starting
Trace 5
FWI
40 m thick
G
NRMS: 3.70%
NRMS: 8.34%
True
Starting
FWI
Depth (m)
Velocity (m s^{-1})
Starting
FWI
% Error
% difference
H
Reflections
Time (s)
Amplitude of first matched, and second not
First Reflection
Second Reflection
I
Starting
FWI
True
Starting
FWI
Starting
Trace 5
FWI
80 m thick
J
NRMS: 3.79%
NRMS: 8.74%
True
Starting
FWI
Depth (m)
Velocity (m s^{-1})
Starting
FWI
% Error
% difference
K
Reflection
Time (s)
Reflection
Reflection shape matched but not fully fitted
L
Starting
FWI
True
Starting
FWI
Starting
Trace 5
FWI

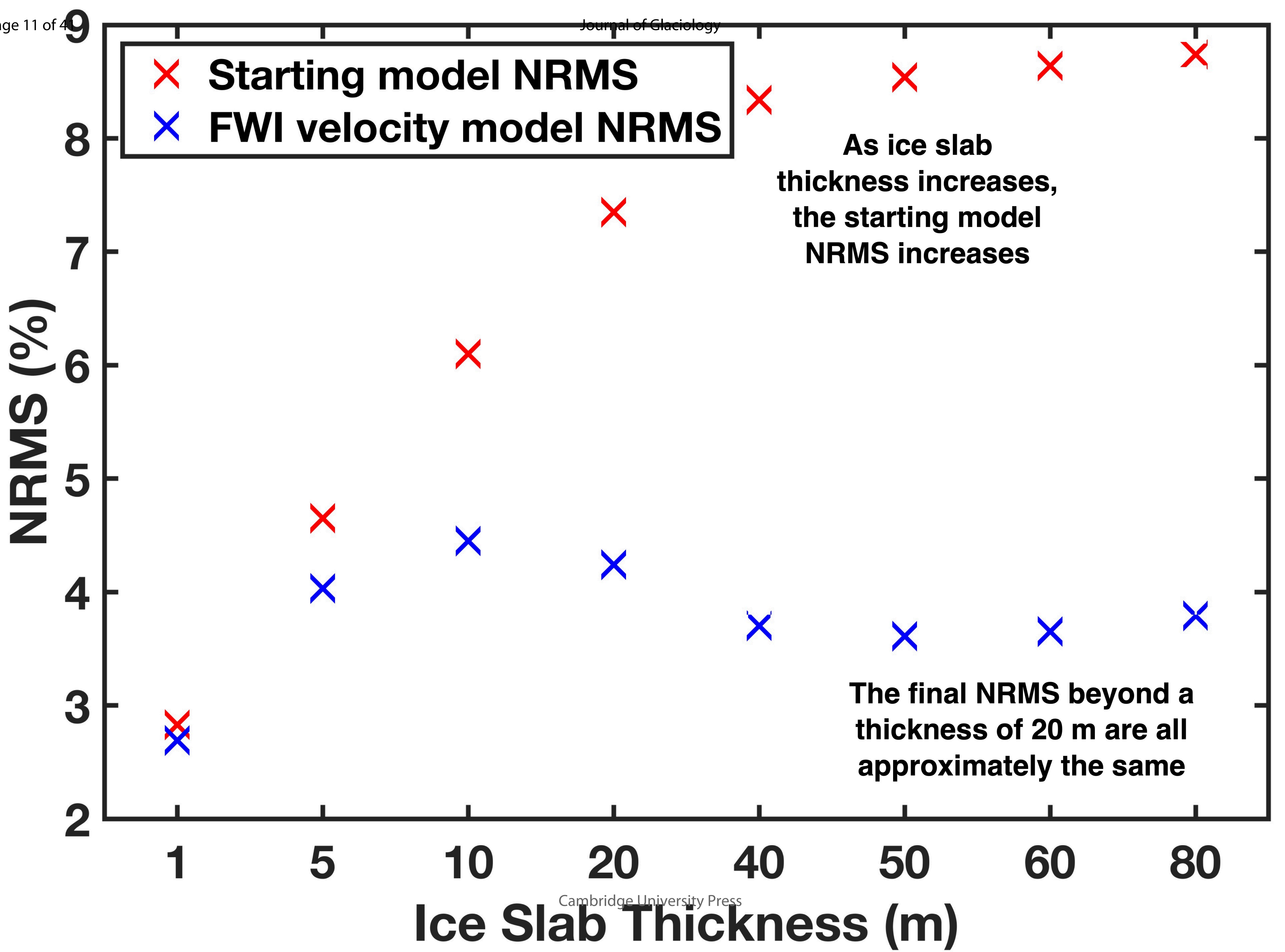

Starting model NRMS
FWI velocity model NRMS
As ice slab thickness increases, the starting model NRMS increases
The final NRMS beyond a thickness of 20 m are all approximately the same
NRMS (%)
2
3
4
5
6
7
8
9
1
5
10
20
40
50
60
80
Ice Slab Thickness (m)

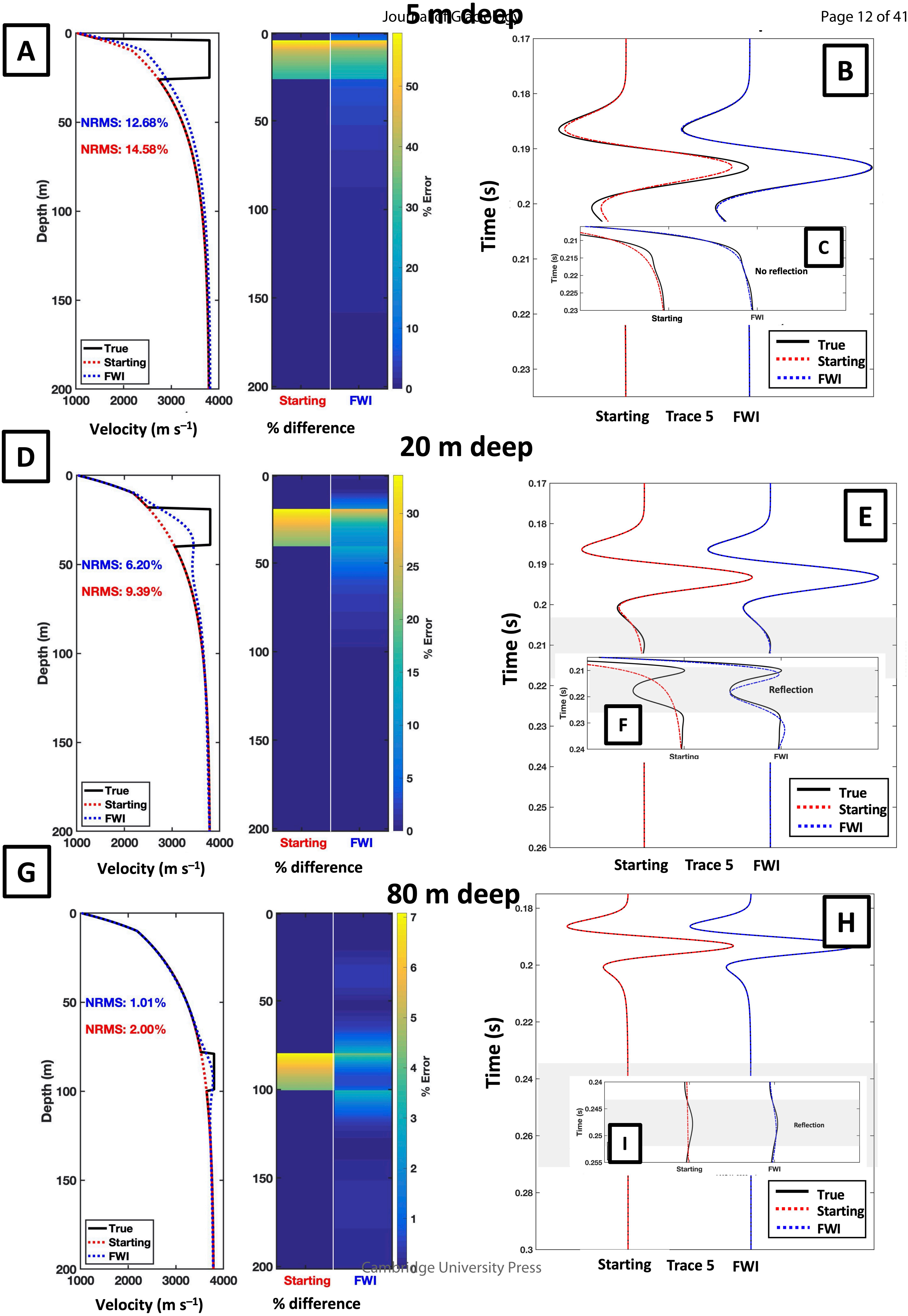
5 m deep
A
B
C
Depth (m)
Velocity (m s⁻¹)
NRMS: 12.68%
NRMS: 14.58%
True
Starting
FWI
% difference
% Error
Time (s)
No reflection
Starting
Trace 5
FWI
20 m deep
D
E
F
NRMS: 6.20%
NRMS: 9.39%
Reflection
80 m deep
G
H
I
NRMS: 1.01%
NRMS: 2.00%
Reflection

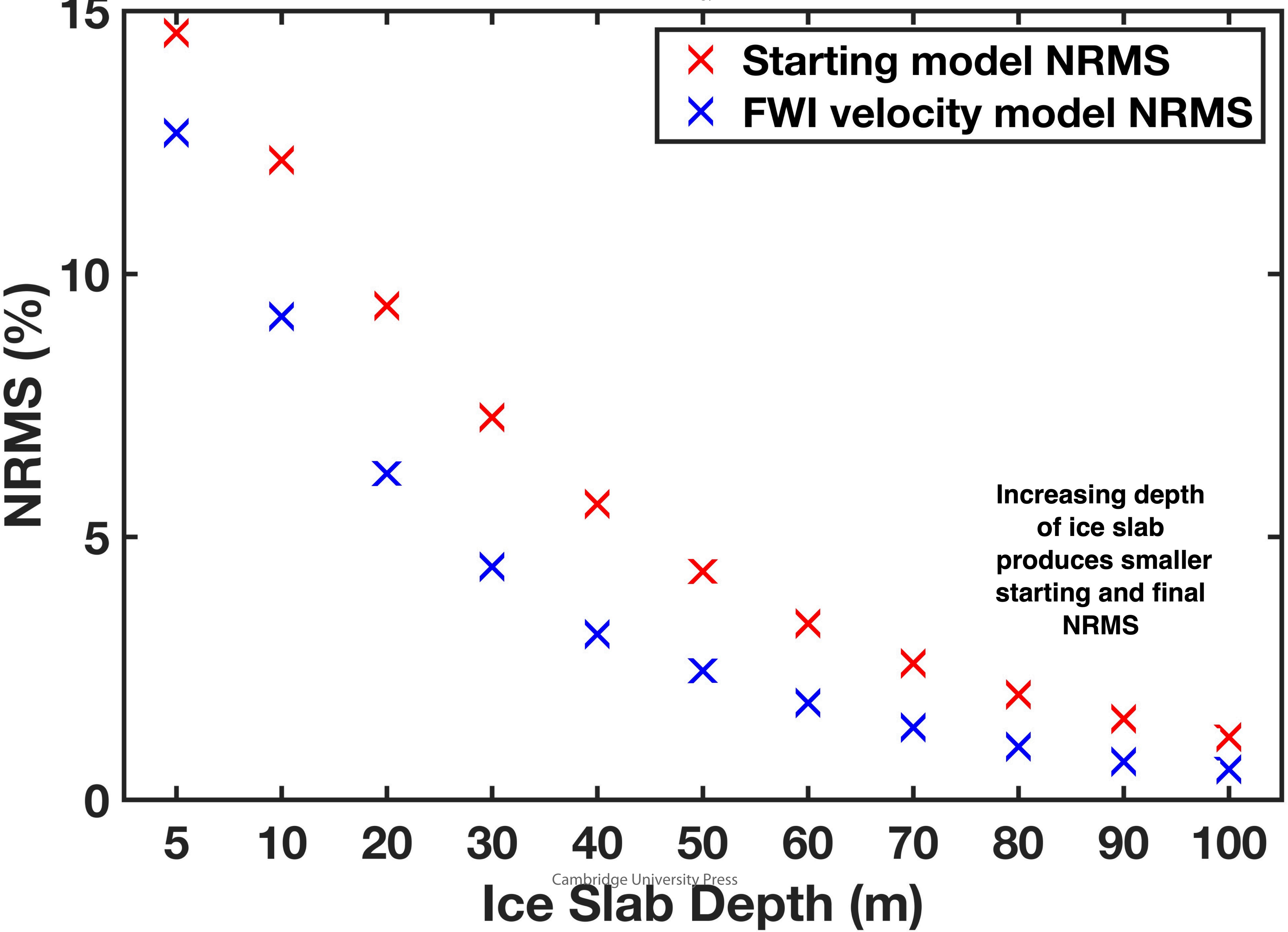
15
10
5
0
NRMS (%)
Starting model NRMS
FWI velocity model NRMS
Increasing depth of ice slab produces smaller starting and final NRMS
5
10
20
30
40
50
60
70
80
90
100
Ice Slab Depth (m)

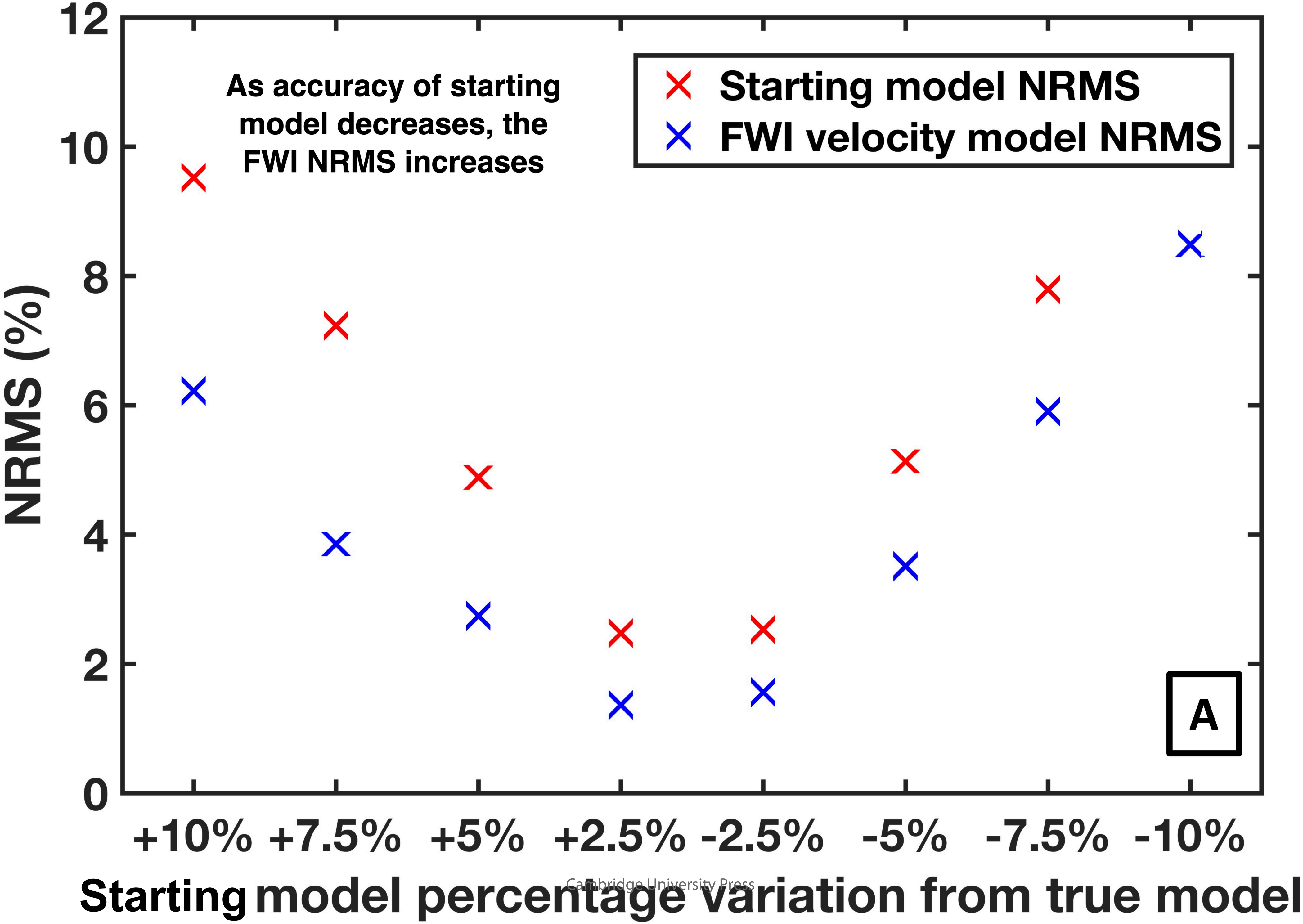
12
10
8
6
4
2
0
NRMS (%)
As accuracy of starting model decreases, the FWI NRMS increases
Starting model NRMS
FWI velocity model NRMS
A
+10%
+7.5%
+5%
+2.5%
-2.5%
-5%
-7.5%
-10%
Starting model percentage variation from true model

Characterising Ice Slabs in Firn Using Seismic Full Waveform Inversion

Emma PEARCE[1,2]*, Adam D BOOTH[1], Sebastian ROST[1], Paul SAVA[3], Tuğrul Konuk[3], Alex BRISBOURNE[4], Bryn HUBBARD[5], Ian JONES[6]

1.School of Earth and Environment, University of Leeds
2. Now at: Ecole et Observatoire des Sciences de la Terre, Institut Terre et Environnement de Strasbourg
3. Department of geophysics, Colorado School of Mines, Golden
4. British Antarctica Survey, Natural Environmental Research Council
5. Department of Geography and Earth Sciences, Aberystwyth University
6: BrightSkies Geoscience

Abstract

The density structure of firn has implications for hydrological and climate modelling, and ice shelf stability. The structure of firn can be evaluated from depth models of seismic velocity, widely obtained with Herglotz-Wiechert Inversion (HWI), an approach that considers the slowness of refracted seismic arrivals. However, HWI is strictly appropriate only for steady-state firn profiles and the inversion accuracy can be compromised where firn contains ice layers. In these cases, Full Waveform Inversion (FWI) may yield more success than HWI. FWI extends HWI capabilities by considering the full seismic waveform and incorporates reflected arrivals. Using synthetic firn density profiles, assuming both steady- and non-steady-state accumulation, we show that FWI outperforms HWI for detecting ice slab boundaries (5-80 m thick, 5-80 m deep) and velocity anomalies within firn. FWI can detect slabs thicker than one wavelength (here, 20 m, assuming a maximum frequency of 60 Hz) but requires the starting velocity model to be accurate to ±2.5%. We recommend for field practice that the shallowest layers of velocity models are constrained with ground-truth data. Nonetheless, FWI shows advantages over established methods, and should be considered when the characterisation of firn ice slabs is the goal of the seismic survey.

1. INTRODUCTION

Meltwater processes on Antarctic ice shelves are influenced by the permeability of surface snow and firn. Ponding of meltwater above impermeable shallow ice has been implicated as a precursor to ice shelf collapse (Banwell 2017). Understanding the extent of impermeable zones within firn - so-called 'ice slabs' - is therefore important for hydrological modelling and subsequent predictions of the long-term stability of the ice shelves that fringe Antarctica. The formation and subsequent freezing of meltwater on (and within) ice shelves reduces firn permeability, causing the formation of surface meltwater ponds (Munneke and others, 2014; Bevan and others, 2017). These in turn influence ice shelf stability by promoting hydrofracture, a process that has been associated with the 2002 collapse of Larsen B ice shelf (Scambos and others, 2004). As ice shelves buttress ice streams, they restrict the transfer of ice from terrestrial ice sheets into the ocean. When the buttressing is removed following collapse, feeder glaciers and ice streams accelerate and can increase the contribution of terrestrial glaciers to sea-level rise (Wuite and others 2015). As patterns of melt and refreezing change (Rintoul and others, 2018), it is expected that the presence of ice slabs within snow-covered regions will become more prevalent, including in Antarctica. There is therefore an important and growing need to characterise ice slabs within firn.

Ice slabs form over several cycles of thaw and refreeze, when pre-existing ice layers within firn coalesce. Ice slabs form in locations where surface melt occurs, including the coastal regions of Antarctica and Greenland. With a lateral extent of tens-to-hundreds of meters, ice slabs make the shallow firn column impermeable (Benson, 1962; MacFerrin and others, 2019, Miller and others 2022) and can increase its local density from 400 – 800 kg m^{-3} (typical of firn) to that of pure glacier ice, 917 kg m^{-3} (e.g. Hubbard and others, 2016; MacFerrin and others 2019; Culberg, and others 2021). Radar data from IceBridge AR flight lines from 2010–2014 show that ice slabs covered 64,800–69,400 km^2 of the Greenland ice sheet in 2014, approximately 4% of the ice sheet's total area (MacFerrin and others, 2019). Greenland's ice slabs have been predicted to increase in area by 130-850% by 2100 depending on the level of 21st century CO_2 emissions (MacFerrin and others, 2019). Without explicitly accounting for the effects of ice slabs, meltwater runoff can be underestimated, for example in Greenland, regional climate models suggest runoff to be underestimated by almost 60% if ice slab formation is excluded (MacFerrin and others 2019; Lai and others, 2020).

Seismic reflections and refractions in ice are caused by any process that changes its elastic properties, including density, bulk and shear moduli, viscosity and anisotropy (Diez and others, 2013; Schlegel and others, 2019), which in turn modify the velocity of compressional (P) and shear (S) seismic energy (Aki and Richards, 2002). Consequently, seismic methods have broad applicability in glaciology for imaging the internal and underlying structure of glaciers and ice masses, (e.g., Brisbourne and others, 2019; Church and others, 2019; Diez and others. 2016; Riverman and others, 2019), but are increasingly used to quantify glacier physical properties (e.g. density, water content, etc.; Booth and others, 2012; Endres and others, 2009; Macchioli- Grande and others, 2020; Peters and others, 2012), temperature from changes in anisotropy (e.g. Llorens and others, 2020; Lutz and others, 2019) and characterise the properties of snow and firn from seismic data (e.g. Bradford, 2010; Diez and others, 2014; Kinar and Pomeroy, 2007; Kohnen and Bentley, 1973; Schlegel and others, 2019).

Seismic methods have been applied to characterise the density structure of firn, using seismic velocity as a proxy for density (e.g., Kirchner and Bently 1979, King and Jarvis 1991, 2007; Booth and others, 2013; Hollmann and others 2021). As the degree of firn compaction increases, so too do density and elastic moduli, leading to an increase in seismic velocity. When an ice slab is present within a firn column, the contrast in seismic velocity between that ice and the adjacent firn can be used to diagnose the presence, bulk properties and thickness of that ice slab.

A commonly used approach for characterising seismic velocity trends in firn from controlled-source seismic data is the Herglotz-Wiechert inversion (HWI) (Herglotz, 1907; Wiechert, 1910; Slichter, 1932; Nowack, 1990) in which a velocity-depth model is evaluated from the slowness (the reciprocal of velocity) of seismic arrivals (e.g. Rege and Godio, 2011; Diez and others, 2013; Thiel and Ostenso, 1961). Though popular in glaciology, a key assumption in HWI is that seismic velocity must increase with depth, which is violated when ice slabs are present in the firn column – specifically across the lower boundary of the slab (or multiple slabs), where material transitions back into unmodified firn. When HWI is applied to regions with ice slabs, slab boundaries are improperly represented due to the limitations of the technique, leading to an incorrect velocity structure above, within and below the ice slab (Aki and Richards 2002).

These limitations can be overcome by the use of seismic Full Waveform Inversion (FWI) methods. FWI extends the capacities of HWI by using both the slowness and amplitude information in the seismic dataset, thereby matching the recorded seismic wavefield rather than just the travel-time of arrivals. For the case of ice slabs, which present a seismic velocity reduction at their base, FWI is in principle sensitive to this velocity structure and hence offers the potential to determine slab thickness. Furthermore, HWI methods consider only the travel-time of first-arrivals in a seismic dataset, whereas FWI can also access later refracted arrivals and the reflections from the bounding interfaces of the ice slabs.

Unlike ray-based methods, which consider only the traveltime of first arrivals, FWI considers finite-frequency wave propagation and evaluates velocity models using the amplitude and travel time of the recorded wavefield. Therefore, the resolution of FWI is only limited by the source and receiver distribution, noise level and scales with the seismic wavelength (Williamson, 1991; Schuster, 1996; Pratt and others 2002, Warner and others, 2013).Babcock and Bradford (2014) provided the first glaciological application of FWI to characterise subglacial seismic velocities in the presence of seismically 'thin' layering (i.e., less than ¼ wavelength, typically ~10 m; Smith, 2007; Booth and others, 2012; Widess, 1973)._ The study reported encouraging results, in particular in terms of improving the accuracy of recorded compressional (P-) wave velocities.

Here, we explore the scope of FWI methods to recover firn velocity structures that are currently unresolvable with HWI . We first compare FWI and HWI for synthetic seismic data that model steady-state firn accumulation profiles, where HWI results should be reliable. The performance of FWI is then considered for seismic velocity models corresponding to firn with ice slab inclusions.

For steady-state firn cases, we show that outputs from FWI are no less accurate than conventional HWI, but are greatly superior for any non-steady state firn profile in which ice slabs are present.

2. INVERSION APPROACHES

2.1 Herglotz-Wiechert Inversion

HWI produces a 1-D velocity structure in which velocity must increase with depth. In the case of firn, this can be used to produce accurate velocity models for steady-state conditions, and has been used repeatedly to characterize firn structure in a variety of settings (e.g., Rege and Godio, 2011; Diez and others, 2013; Thiel and Ostenso, 1961). This one dimensional continuous velocity structure can be approximated by a stack of thin layers of constant velocity, which can be considered a suitable approximation for many firn structures. Following Snell's law, seismic energy incident at a boundary refracts and the ratio of the sine of the angle of incidence θ_n and the velocity in the n^{th} layer, v_n is constant, defining the horizontal slowness or ray parameter p.
For a monotonically increasing velocity, the ray parameter decreases monotonically, causing the ray to turn and to be recorded at the surface allowing sampling of the velocity structure. At the turning point, where the maximum depth (z_{max}) of the propagation is reached, the refraction angle θ reaches 90^o and the horizontal slowness is equal to the inverse of the velocity at this depth, allowing a mapping of seismic velocities using methods such as HWI.

To convert slowness to a depth/velocity domain, the HWI approach uses Abel's integral equation. From Bôcher (1909), the necessary and sufficient conditions that Abel's integral must meet are that the derivative of t(*x), slowness,* can be discontinuous, but t*(x)* itself cannot be discontinuous (such as when dealing with velocity discontinuities and lateral velocity variations). For the travel time-offset data to be used successfully with the HWI , the travel time picks obtained from the first break arrival times of the seismic data must be smooth and continuous. Various algorithms exist for fitting a curve to the first break picks to achieve this, with the Levenberg-Marquardt algorithm being used here (Moré, 1978; Kirchner and Bentley, 1990), as implemented by King and Jarvis (2007). The traveltime, *t*, approximation is achieved through

$$t = a_1\left(\left(1 - e^{-a_2 x}\right) + a_3\left(1 - e^{-a_4 x}\right) + a_5 x\right) \qquad (1)$$

with $a_{1\text{-}4}$ being curve fitting parameters and a_5 is the inverse of the seismic velocity of ice.

Using Eq (1) instead of the measured traveltimes ensures that traveltime increases monotonically with distance, (i.e. velocity increases monotonically with depth), and allows a solution using Abel's equation (Kirchner and Bentley, 1990). For each offset (x), the slowness (p) of the traveltime curve can be determined and the depth (z) to the related velocity (as slowness u) can be determines using:

$$z(u) = \frac{1}{\pi}\int_0^{x(u)} cosh^{-1}\left(\frac{p}{u}\right)dx \qquad (2)$$

Once repeated for all offsets on the slowness offset curve, a smooth velocity-depth model is obtained (Nowack, 1990; Aki and Richards 2002).

2.2 Full Waveform Inversion

FWI delivers subsurface velocity models by minimising the misfit between observed and modelled seismic waveform data. The seismic wave equation is used to describe wave propagation in a medium and can be used to calculate synthetic seismic waveforms (**p'**) from a (starting) velocity model, (Virieux and Operto, 2009; Babcock and Bradford, 2014). The starting velocity model is updated through successive iterations that improve the match between predicted and observed data.

A solution to the inversion is found by matching the predicted seismic data (**p'**) to the observed data (**d**) trace by trace (Mulder and Plessix, 2004; Warner and others, 2013). This uses a non-linear local iterative minimisation scheme: in its simplest form, the misfit is characterised by a scalar value termed the objective function (Warner and others, 2013). The most common form of the objective function (OF) is a least-squares (LS) formulation that minimises the sum of the square of the difference between the observed and predicted datasets:

$$f = \frac{1}{2}|\boldsymbol{p}' - \boldsymbol{d}|_2^2 \qquad (3)$$

where $|\ |^2$ indicates the L2 (least-squares) norm. The model that minimises the objective function is considered to the best solution to the inversion (Pratt, 1999).

The FWI algorithm used in this study is based on the acoustic wave equation,

$$\frac{\partial^2 \boldsymbol{p}}{\partial t^2} = v_p^2 \rho \nabla . \left(\frac{1}{\rho} \nabla \boldsymbol{p} \right) \qquad (4)$$

where **p** is pressure, v_p is the propagation velocity of seismic compressional (P-) wave, and ρ is the density of the medium. The equation assumes isotropic wave propagation and no attenuation.

The acoustic wave equation is usually modelled with finite-difference (FD) methods, due to their simplicity and efficiency compared to other techniques available to solve partial differential equations (Virieux and Operto, 2009; Zhang and Yao, 2013). To simplify the source characterization in the FD approach the source wavelet is modelled using a Ricker wavelet with a peak frequency of 60 Hz. To ensure modelling stability, data are recorded with a time sampling of 0.001 s, for 1 second of propagation (Courant and others., 1967).

Seismic wave propagation is described by the seismic wave equation containing the elastic properties of the subsurface. For relatively simple elastic (velocity) models, the seismic wave equation can be solved analytically. For more complex models, numerical solutions are necessary (Ben-Menahem and Singh, 2012; Guasch, 2012; Moczo and others, 2014). FD is a commonly used and stable method and has been found to provide computationally efficient and accurate solutions for a wide range of velocity structures (Virieux and Operto, 2009; Zhang and Yao, 2013).

FWI solutions can suffer from non-linearity and model non-uniqueness, and the technique can be computationally expensive. A particular problem is that of cycle-skipping, where modelled and recorded data are out of phase by half a wavelength, yet still offer a locally-minimised objective function (Sirgue, 2006) (Figure 1). In such cases, FWI converges on a local, rather than global, minimum, which reduces the objective function but produces, an incorrect velocity model. Cycle skipping can be exacerbated by data acquisition, survey geometry and the choice of inversion algorithm (Guasch, 2012; Shah and others, 2012; Jones, 2015, 2019; Brittan and others, 2013; Bai and Yingst, 2014; Borisov and others, 2017) and starting velocity model, which is selected carefully such that the first iteration of modelled data matches the observations to within half a wavelength. The risk of cycle skipping is mitigated by i) using the low frequencies (i.e., long wavelengths) in the data which, due to their longer wavelength, are less prone to cycle skipping, and ii) including far-offset data, which typically contain higher velocities and thus longer wavelengths (Warner and others, 2013; Sirgue and others, 2009; Al-Yaqoobi, 2013; Virieux and Operto, 2009).

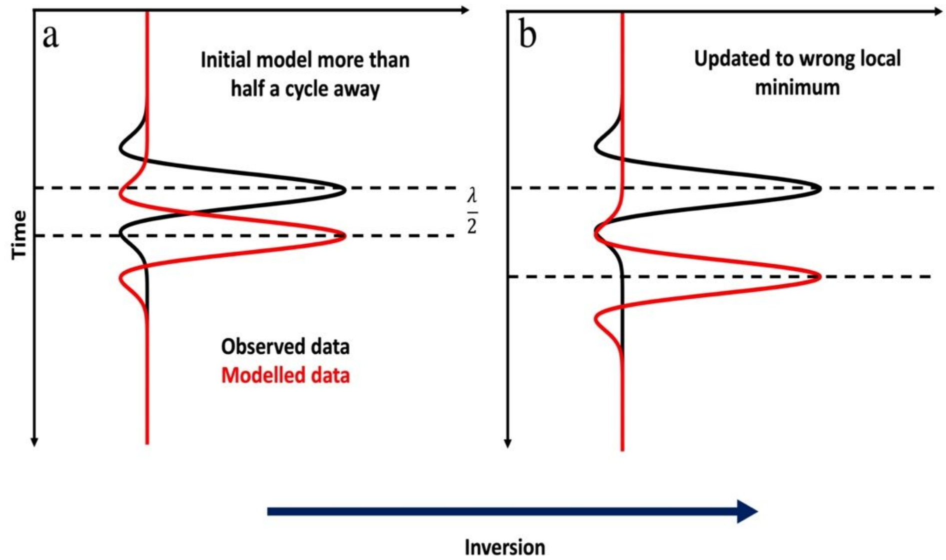

Figure 1: Schematic representation of cycle skipping (adapted from Prajapati and Ghosh, 2016). (A) If the initial modelled data and observed data are more than half a cycle away then (B) the data updates to a local minimum, i.e., the modelled data is matched to the incorrect part of the observed data, in that the trailing-trough of the black curve coincides with the leading-trough of the red curve

For the inversion, seismic propagation is modelled assuming an acoustic wave in a 2-D isotropic medium with no attenuation, with the recovered parameter being P-wave velocity. When calculating the residual, data are normalised by the maximum amplitude in each trace.

The misfit between recorded and modelled data is defined as the objective function (OF) given in Eq. 3. We use an adjoint method (Plessix, 2006) and a gradient-based method (Tarantola, 1988) to update the model between iterations. We use the Madagascar framework (Fomel and others, 2013), provided by the Center for Wave Phenomena, to implement this approach (Aragao and Sava, 2020). To minimize the impact of cycle skipping, we start iterations for the low frequency wavefield, filtered between 3 Hz and 10 Hz, until OF updates suggest model convergence. Thereafter, the frequency content is progressively increased in 10 Hz bands, to a maximum of 60 Hz.

In our FWI we use a gradient approach to define the fit between recorded and modelled data. To minimise the OF with respect to the model parameters (**m**) the OF is differentiated,

$$\Delta \mathbf{m} = -\alpha \frac{\partial f}{\partial \mathbf{m}} \tag{5}$$

This OF gradient indicates the direction of update of the model **m** in the next iteration in order to reduce the OF, with α a scaling factor known as the step length (Dai and Yuan 1999).

3. SYNTHETIC TESTING OF FWI APPLICABILITY

To validate the performance of FWI for realistic steady-state firn velocity profiles, firn density profiles are simulated using the Herron-Langway (HL) firn densification model (Herron 1980) and converted to velocity (Kohnen, 1972). The HL model is based on the three stages of firn generation and uses snow accumulation rate and ambient temperature as input variables.

The HL model requires parameters to be chosen for total firn thickness, surface accumulation rate, surface snow density, and the average temperature at 10 m depth. The chosen values (Table 1) for density (snow, ice and critical), and temperature are consistent with those of Herron and Langway (1980).

Table 1: Parameterisation used for the Herron and Langway firn densification model

Model Parameter	Value
10 m depth temperature	-30 ^{o}C
Density of pure ice	917 kg m^{-3}
Density of surface snow	400 kg m^{-3}
Depth of model	200 m
Critical density	550 kg m^{-3}
Accumulation rate	0.2 m w.e. yr^{-1}

The accumulation value of 0.2 m w.e. yr^{-1} is used to represent a typical value for coastal Antarctica. It is generally accepted that higher accumulation rates produce thicker firn profiles, and thus gentler gradients of density and velocity increase (Herron and Langway, 1980) (Figure 2).

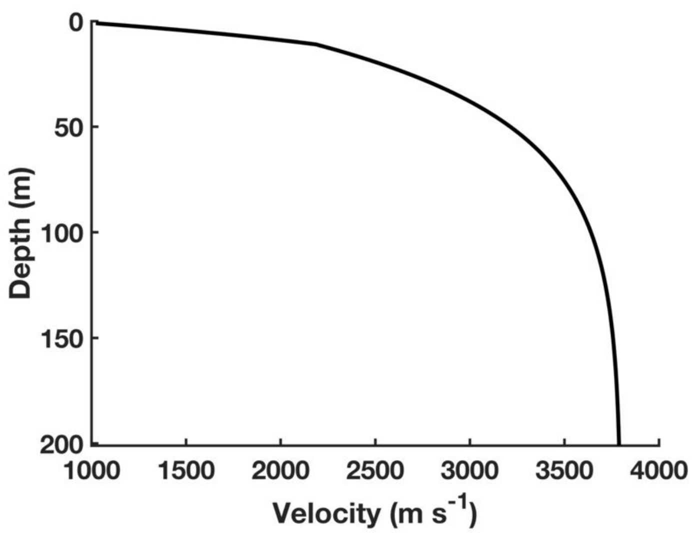

Figure 2: The synthetic seismic velocity profile obtained by converting the Herron and Langway densification profile with an accumulation rate of 0.2 m w.e. yr^{-1} with the Kohnen (1972) approximation. From a depth of 0 to 25 m, the most gradual increase in velocity with depth is seen. Deeper than 25 m (where the critical density

is reached) the densification, and hence velocity, rate increases. A maximum velocity of 3800 m s^{-1} is reached at 200 m depth.

The density profiles obtained from the HL model are converted to seismic velocity using the Kohnen (1972) approximation. A single seismic source is placed at 0 m offset, with surface receivers placed from 0 - 1000 m (5-times greater than the model depth) in one meter increments.

Three analyses are performed using the synthetic firn velocity profiles. Firstly, the velocity model from the FWI is compared to the velocity model produced by the HWI , where the HWI model is used as the starting model for FWI. Secondly, we impose an increasing degree of systematic error to the true model to use as the starting velocity model for the FWI, to explore the extent to which FWI can resolve incorrect starting models. This will explore how a decreasing starting model accuracy affects the FWI update to the velocity model and the data. Finally, the third model simulates two different HL firn densification profiles (low and high accumulation of 0.1 m w.e. yr^{-1} and 0.4 m w.e. yr^{-1}, respectively), but uses the starting velocity model from the original profile (an accumulation of 0.2 m w.e. yr^{-1}). This explores whether FWI can distinguish different densification scenarios even when a 'benchmark' starting velocity profile is assumed.

Thereafter, the steady-state models are modified to introduce ice slabs into the firn profile. Assuming the velocity and density of an ice slab to be 917 kg m^{-3} and 3800 m s^{-1} (Paterson, 2016), these values are allocated to varied depth and thickness ranges of the firn profile to simulate the presence of ice slabs. We assess whether FWI is able to detect the velocity change at the upper and lower interfaces of the slab, and the extent to which it resolves the correct velocity model.

Velocity model outputs from FWI are compared to the true subsurface velocity model using the NRMS error, defined by Kragh and Christie (2002) as

$$NRMS = \frac{200 \times RMS(V - U)}{RMS(V) + RMS(U)} \quad (6)$$

where RMS(V) and RMS(U) are the root-mean-square velocities of the true and predicted. The absolute percentage difference (*DD*) between the true and inverted velocity models is defined throughout the model with a depth interval of one meter. *DD* indicates how close the modelled velocity (Uz_i) is to the true velocity (Vz_i), calculated as;

$$DD = \sqrt{\left(\frac{U_{zi} - V_{zi}}{U_{zi}} \times 100\right)^2} \quad (7)$$

4. RESULTS

4.1 HWI of steady-state profiles

Data are forward modelled from the synthetic velocity model (true model). This produces the observed seismic dataset. From these observed data, travel times are extracted and the HWI inversion is used to obtain an estimation of the subsurface velocity structure and compared to the true velocity model.

In general, HWI provides a close representation of the velocity distribution of the steady-state firn profile. From 15-125 m, the velocity is recreated accurately, and the predicted velocity remains within 3% of the true model. For the shallowest depths, before the critical density is reached, HWI overestimates velocity. This is consistent with observations of Hollmann and others (2021), who suggested that HWI are poorly constrained in the near-surface, with inaccuracies in first-break picking being proportionally greater at smaller travel times. Beyond 125 m depth, HWI underestimates velocity by 4%, converging on a velocity of ~3650 m s^{-1}.

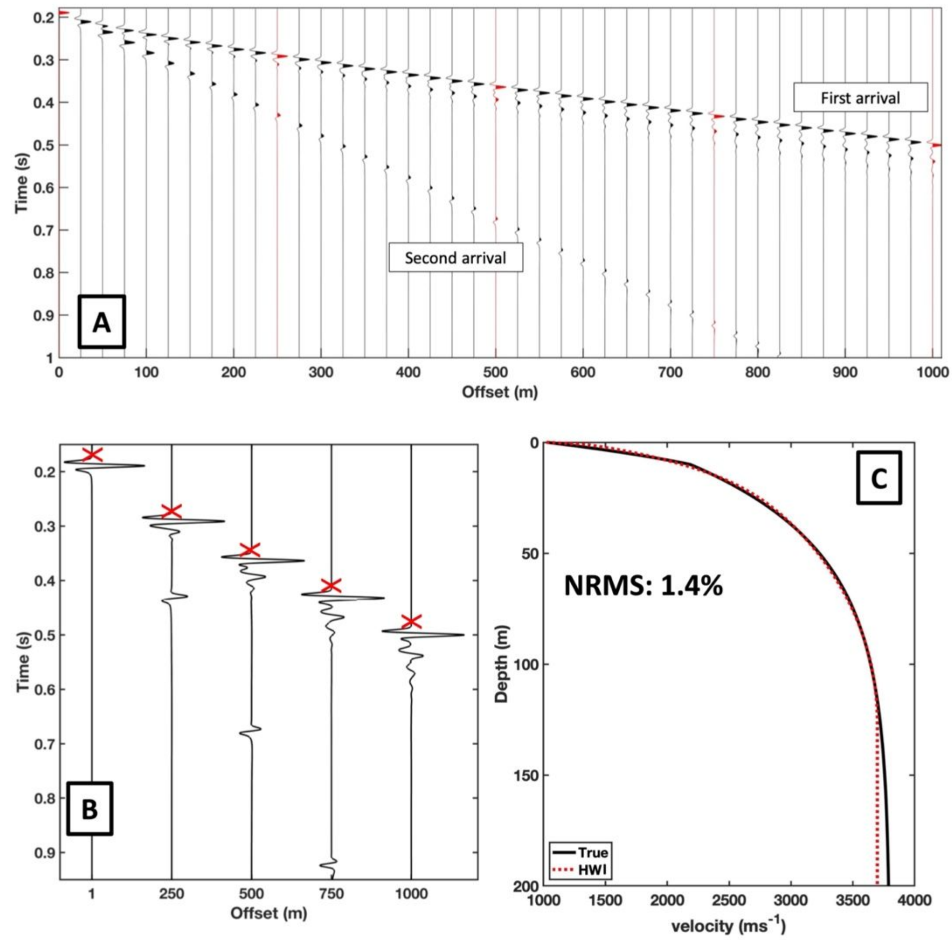

*Figure 3: (A) Forward modelled, observed, synthetic data (**d**). produced from the HL firn velocity model with an accumulation rate of 0.02 m w.e. yr^{-1} . Red traces show those enlarged in (B). (B) First break picks used as the input for Herglotz-Wiechert shown for selected offsets. (C). The output velocity model produced by the HWI (Red) compared to the true HL firn velocity model (Black).*

4.2 FWI of steady-state profiles

The output of the HWI (Figure 3C) is used as a starting velocity model for FWI. Data are forward modelled from this starting velocity model to obtain a predicted seismic dataset, **p'.** Comparing (the observed data (**d**)) and **p'** (Figure 4), the first arrival is modelled accurately but cycle skipping has occurred for the second arrival. This is evident in the red trace in Figure 4A: the second arrival in the predicted data (red) appears ~0.005 s earlier than in the model, suggesting that shallow velocities are being overestimated. This is also evident in Figure 4B, where the red-coloured second arrivals show a faster velocity trend than does the model. This mismatch can propagate into deeper velocity values, and hence requires improvement.

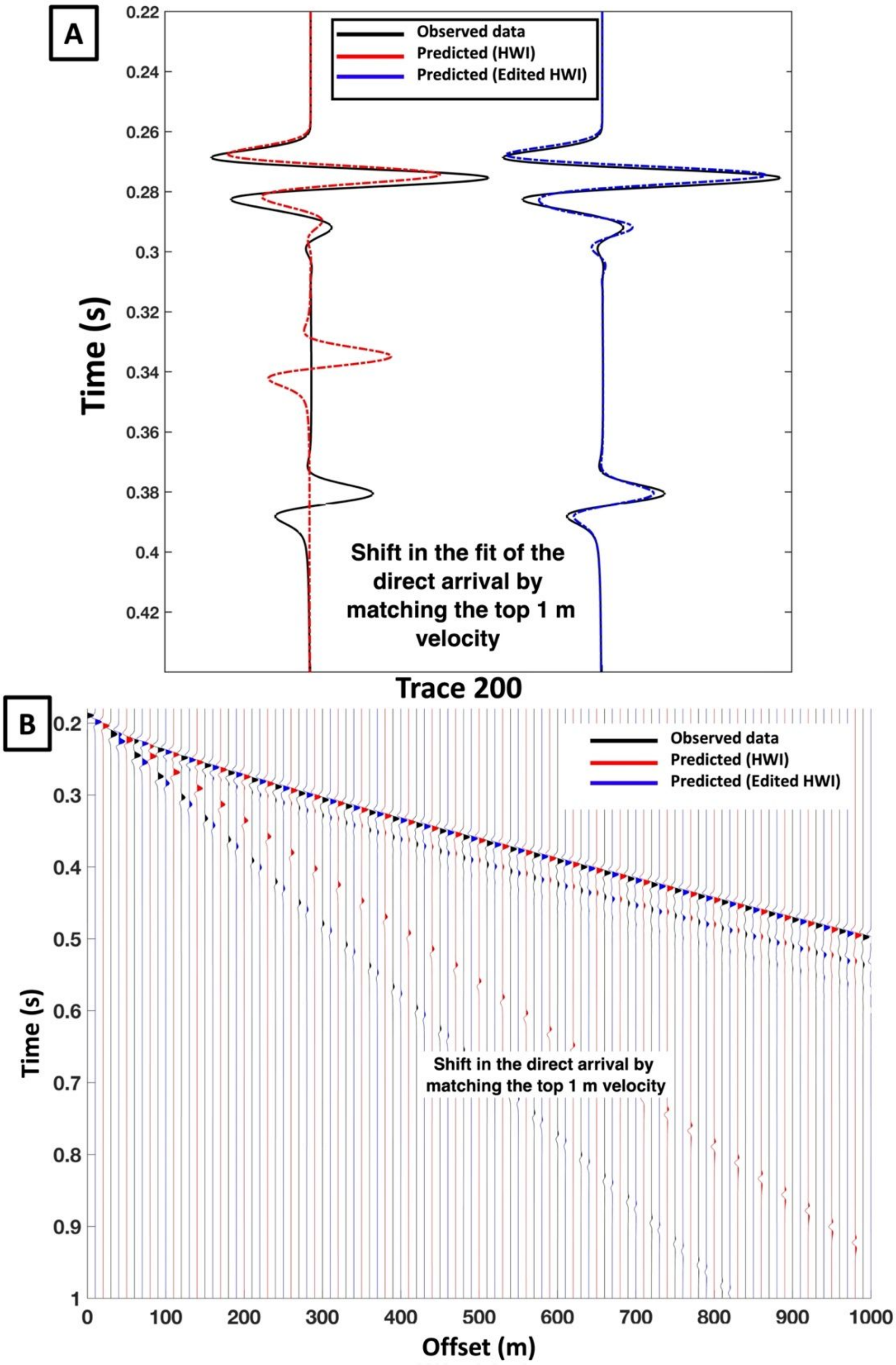

Figure 4: (A) Comparison of seismic arrivals for trace 200 between the observed data (black), the predicted data (red) and predicted data from an adjusted starting velocity model (blue). The data produced from the predicted (HWI) starting model are prone to cycle skipping in the second arrival, hence the edited HWI velocity model is used for a starting model with FWI.

The blue trace in Figure 4A shows the output from a modified starting model, which fixes the velocity in the uppermost one meter of the profile to the true model value (1023 m s^{-1}). With this modification, both arrivals are now free from cycle skipping. This highlights the vulnerability of HWI and FWI to near-surface velocity errors, and points to the need for field acquisitions to constrain the shallowest velocities – either through a small-offset seismic refraction survey or a vertical seismic profile (VSP) in a borehole or test pit.

Once the uppermost velocity is constrained, Figure 5 suggests that FWI can perform as reliably as the HWI that provided the starting model: the NRMS for both approaches is ~1.4%.

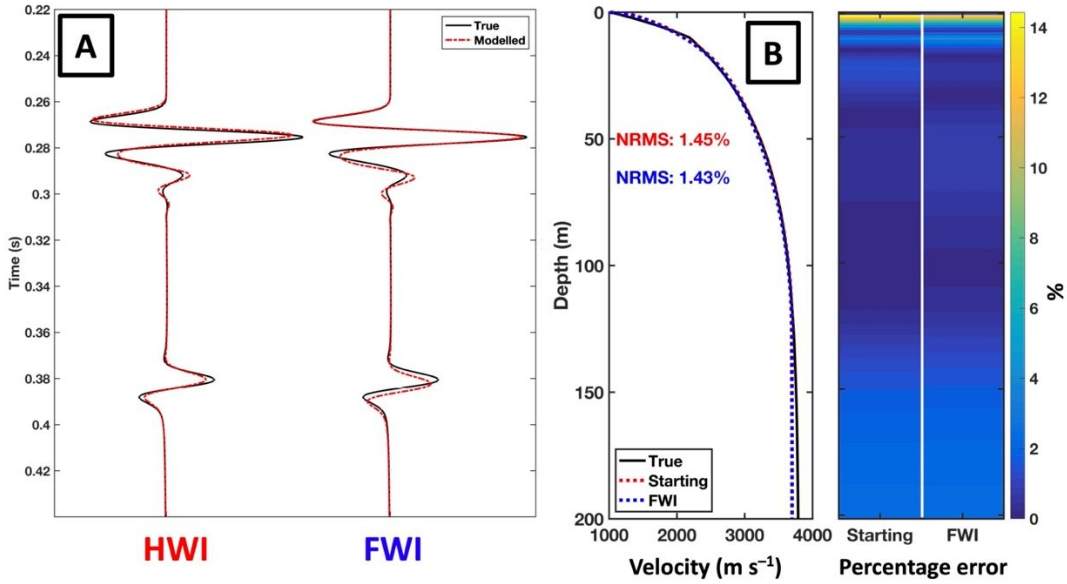

Figure 5: (A) The output of FWI on the adjusted HWI starting model, shown for trace 200. (B) Velocity model output from FWI compared to the starting model (red) and true model (black), expressed as NRMS and the percentage error between the two output models (HWI and FWI) and the true model.

To explore the sensitivity of FWI to velocity errors, the starting velocity model is perturbed from its true value by up to +/- 10%. This generates eight further starting models. Figure 6 shows examples of FWI performance where the starting model is overestimated by 2.5% (A and C) and 10% (B and D). The analysis indicates that FWI is robust for the 2.5% error, but cycle skips for the case of the 10% error (Figure 7).

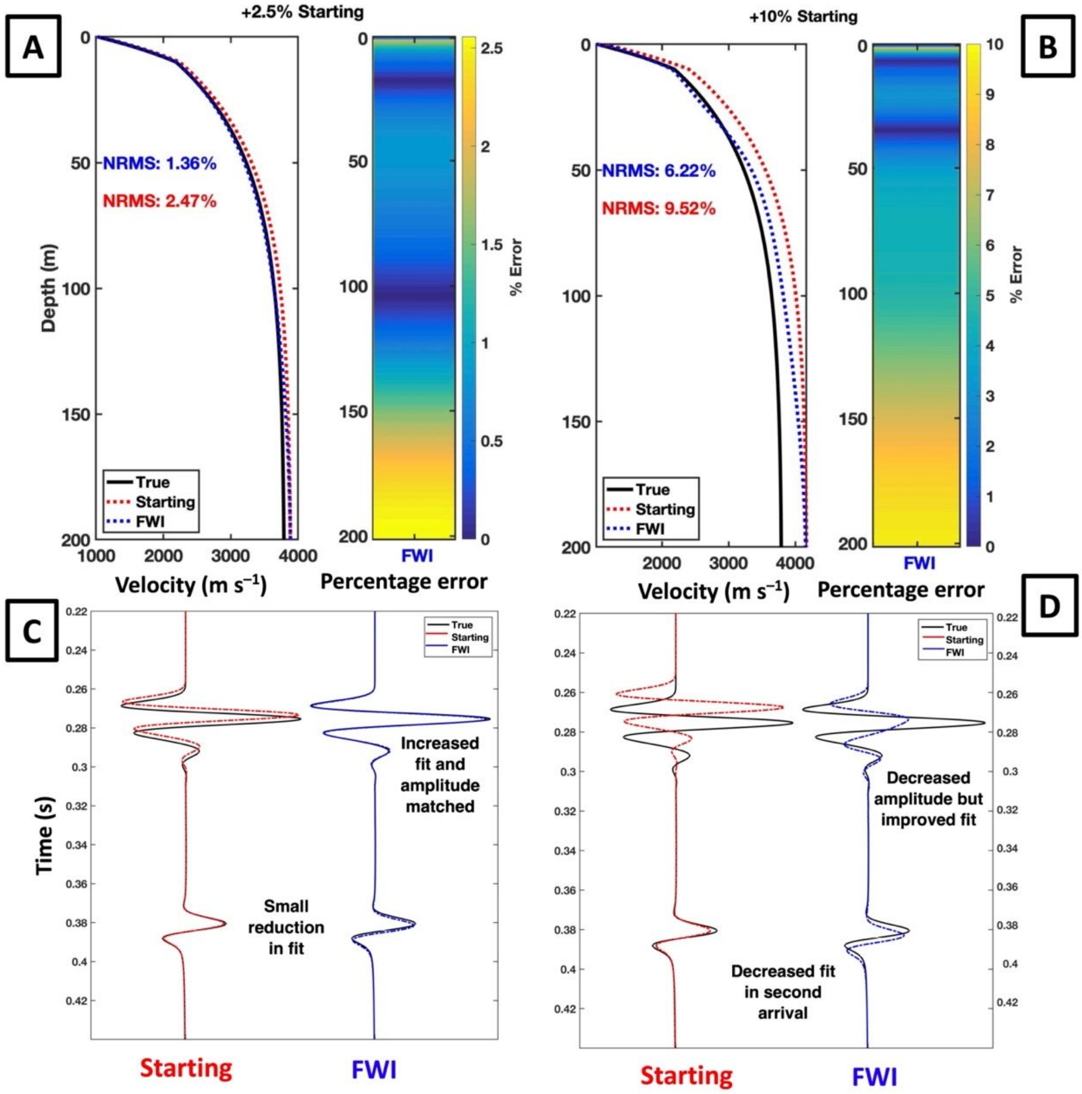

Figure 6: (A) and (B), the velocity models produce by FWI for a starting model that is a 2.5% overestimation and 10% overestimation of the true model. (C) and (D) the seismic data for trace 200 for the same starting models respectively. The over estimation of 10% still enables the near offset traces to be matched, but the amplitude is not correctly accounted for with the acoustic FWI.

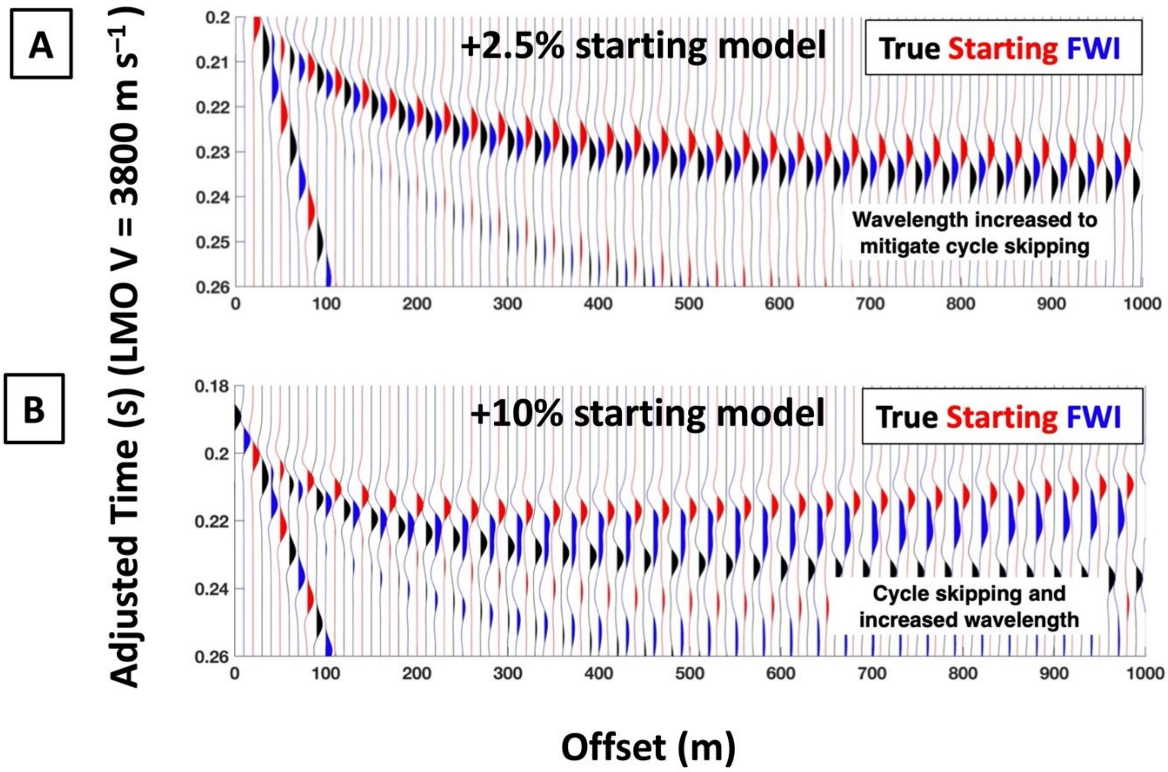

Figure 7: The observed (true), starting (predicted) and updated (FWI) data for (A) a 2.5% starting model and (B) a 10% starting model. The data updated by FWI for the 10% starting model shows cycle skipping from an offset of 300 m. The data update from FWI for 2.5% model shows no cycle skipping, but from an offset of 800 m, the peaks in the data are not fully matched.

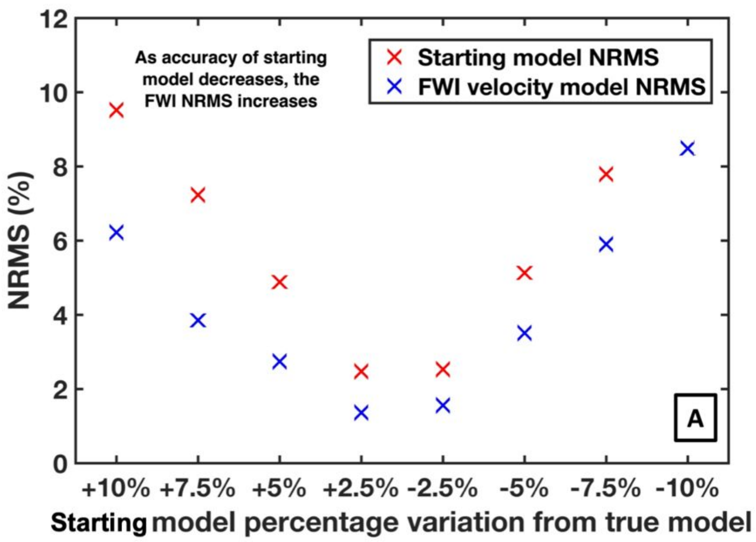

Figure 8: (A) The NRMS update for eight starting model variations. As the perturbation to the starting model increases, the update by FWI is further away from the true model (I.e. a higher final NRMS). FWI is insensitive to whether a starting velocity model is under- or over-estimated, producing similar results for both scenarios.

This perturbation analysis (summarized over Figures 6, 7 and 8) shows that FWI can recover the true velocity model even with an incorrect starting model provided that the deviation does not exceed 2.5%. At larger deviations, the inversion becomes prone to cycle skipping in the far offset traces, and the depth to which a reliable inversion can be performed decreases. This is expected since the absolute mismatch between the starting and true velocity models is less in the shallow surface, where the velocity is smaller. Therefore, for the 60 Hz frequencies used in this study, FWI requires a starting model that is within 2.5% of the true velocity profile to provide reliable results.

4.3 Recovery of a firn profile from an incorrect snow accumulation regime

To determine whether FWI is able to resolve different accumulation regimes, we deliberately misrepresent the starting velocity model with substitute models corresponding to lower and higher accumulation.

When accumulation is over-estimated in the starting model (Figure 9a, c), FWI improves the NRMS error by ~60%. The final NRMS mismatch is 3.5%, although velocities are overestimated in the depth range of 50-150 m, approaching 4000 m s^{-1}. In this range, the starting velocity model is too far from the true model, causing cycle-skipping. However, when accumulation is under-estimated in the starting model (Figure 9b, d), the improvement to the NRMS error is ~77% and the final NRMS mismatch is just 1.4%. These results suggest that FWI is largely robust to errors in an assumed accumulation model, although the starting velocity model should still be as accurate as possible to avoid cycle-skipping.

Combined, these results show the potential for stable FWI implementation for steady-state firn profiles. Although vulnerable to cycle-skipping errors, FWI can recover the seismic velocity structure of firn profiles when supplied with i) a reasonable starting velocity model derived from initial HWI and ii) constraint of the shallowest seismic velocity.

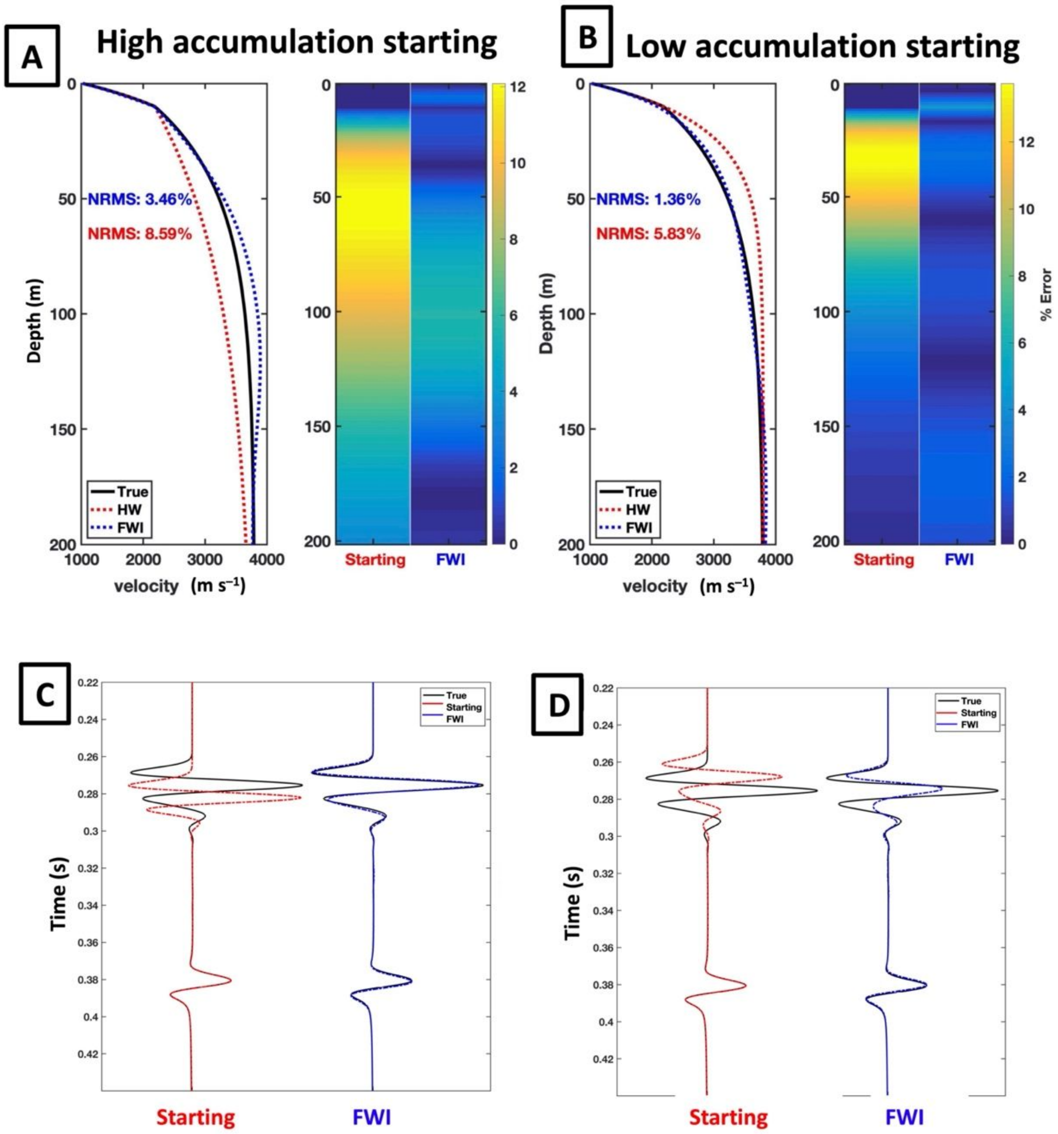

Figure 9: Velocity model outputs from FWI for a starting model that assumes (A) too high an accumulation, and (B) too low an accumulation compared to the true model. (C) and (D) show the seismic data for trace 200, for a starting model from too high and low accumulation respectively.

5 FWI DETECTION OF ICE SLABS

5.1 Thickness variations

In our experiment, the upper boundary of the ice slab is fixed at a depth of 30 m, and its thickness is extended from 5 m to 80 m. Figure 10 shows selected examples of 5 m, 20 m, 40 m and 80 m from this thickness range, and results are summarised in Figure 11.

For any ice slab thickness exceeding the minimum wavelength of the seismic data (here, λ = 20 m) (Figure 10D), FWI models show a distinct deviation towards increased velocity compared to the starting model. Thinner layers cause a perturbation to the FWI velocity model, which could be used to infer the presence of a slab, but they are unable to resolve its thickness or velocity. For the thinnest slab thickness of 5 m (Figure 10 A), neither HWI or FWI are sensitive to the velocity anomaly and the NRMS error is similar in both cases. For thicker ice slabs, particularly >2 λ (40 m) (Figure 10 G), the velocity anomaly is recovered well by FWI: the maximum velocity in the slab is ~3800 m s^{-1}. Furthermore, the velocity also correctly reduces in the undisturbed firn that underlies the slab.

As the ice slab thickness increases, the NRMS error between the true model and the starting model increases. An increase in slab thickness from 1 m to 80 m results in an increase in NRMS reduction from approximately 5% to 60%. (Figure 11). In all cases, ice slabs $\geq$ 40 m (2 λ) thick show a 50%-60% decrease in NRMS while ice slabs thinner than 40 m only reduce NRMS by 5%-27%.

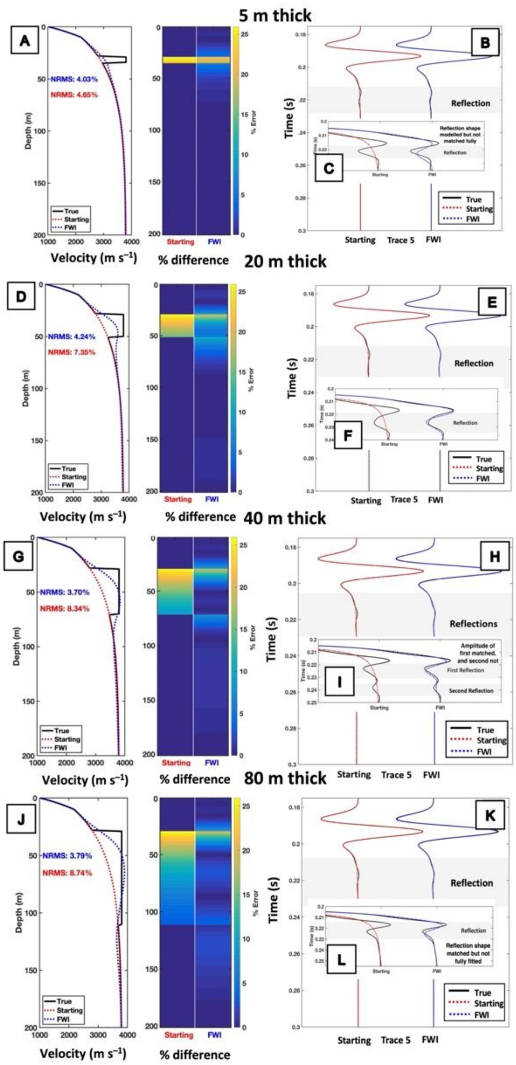

Figure 10: Velocity model outputs from ice slabs of different thickness (A) 5 m, (D) 20 m, (G) 40 m and (J) 80 m. As ice slab thickness increases, the base of the ice slab propagates into firn with a greater compaction, and therefore seismic velocity. As such, the velocity anomaly between the firn and ice slab is smaller at greater depths.

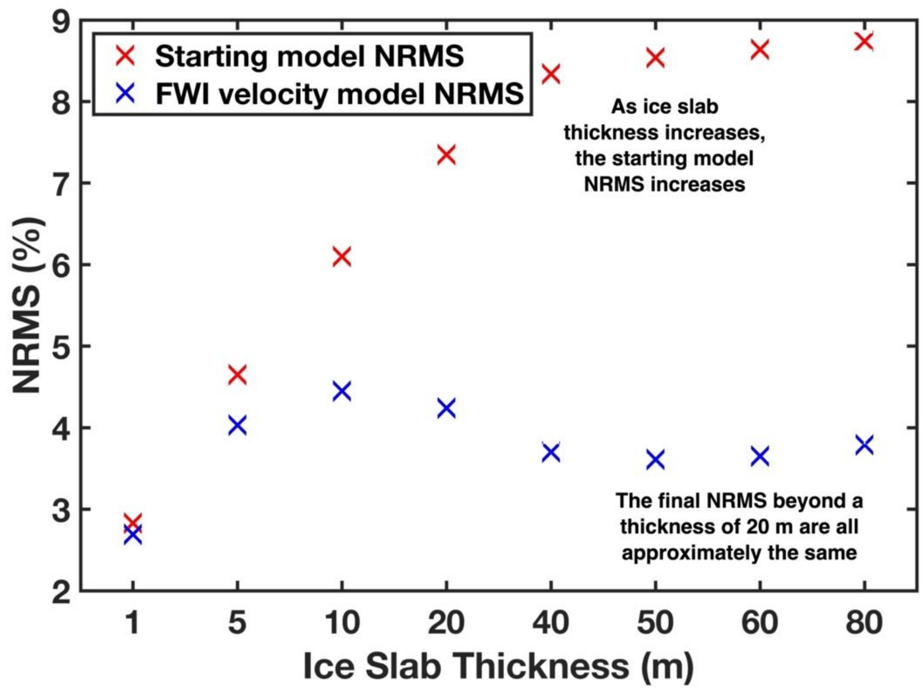

Figure 11: The reduction in NRMS achieved by FWI. An ice slab of greater thickness has the largest starting NRMS error but can be corrected by FWI.

5.2 Depth variations

For these experiments, the thickness of the ice slab is fixed at 30 m, and the depth of its upper boundary is varied from 5 m to 80 m. Figure 12 shows selected examples of 5 m, 20 m and 80 m from this depth range, and results are summarised in Figure 13.

For ice slabs at a depth of 5 m (Figure 12A), no significant improvement to the velocity model is achieved by FWI. For these data, FWI increases the overall velocity of the starting model from a depth of 5 m to 60 m and does not recover the velocity inversion, instead introducing a localised velocity update where the ice slab is located. When the ice slab is located at depths of >=20 m (Figure 12 D and E), a localised update to the starting model is observed, and the velocity inflexion at the base of the ice slab is detected. The precision of the velocity inflexion marking the upper and lower interface of the slab increases with depth, given that the starting model becomes closer to the true model. This is consistent with the performance for the previous models, in which the resolution of thicker ice slabs was improved given the smaller deviation to the starting velocity model. Increasing the slab depth over the full range investigated, from 5 m to 100 m, results in a increase in NMRS reduction from 13% to 51%.

Resolution limitations to detect ice slabs with FWI are based on the minimum wavelength of the seismic data. When ice slabs are present with a thickness similar to the wavelength (20 m), FWI begins to generate a distinctive velocity update, producing an apparent deviation from the starting model and detecting the velocity inversion. As the thickness of the ice layer increases, FWI recovers the true velocity anomaly well, with 40 m (2 λ) thick layers accurately predicting the expected 3,800 m s^{-1}. Layers thinner than the dominant wavelength are still detected by FWI, causing deviations to the recovered velocity model; however, FWI does not recover ice velocities correctly in such cases. Ice slabs located within a depth interval less than the minimum wavelength are recovered as a single ice slab, with increasing distance between the features resulting in improved characterisation of the two layers.

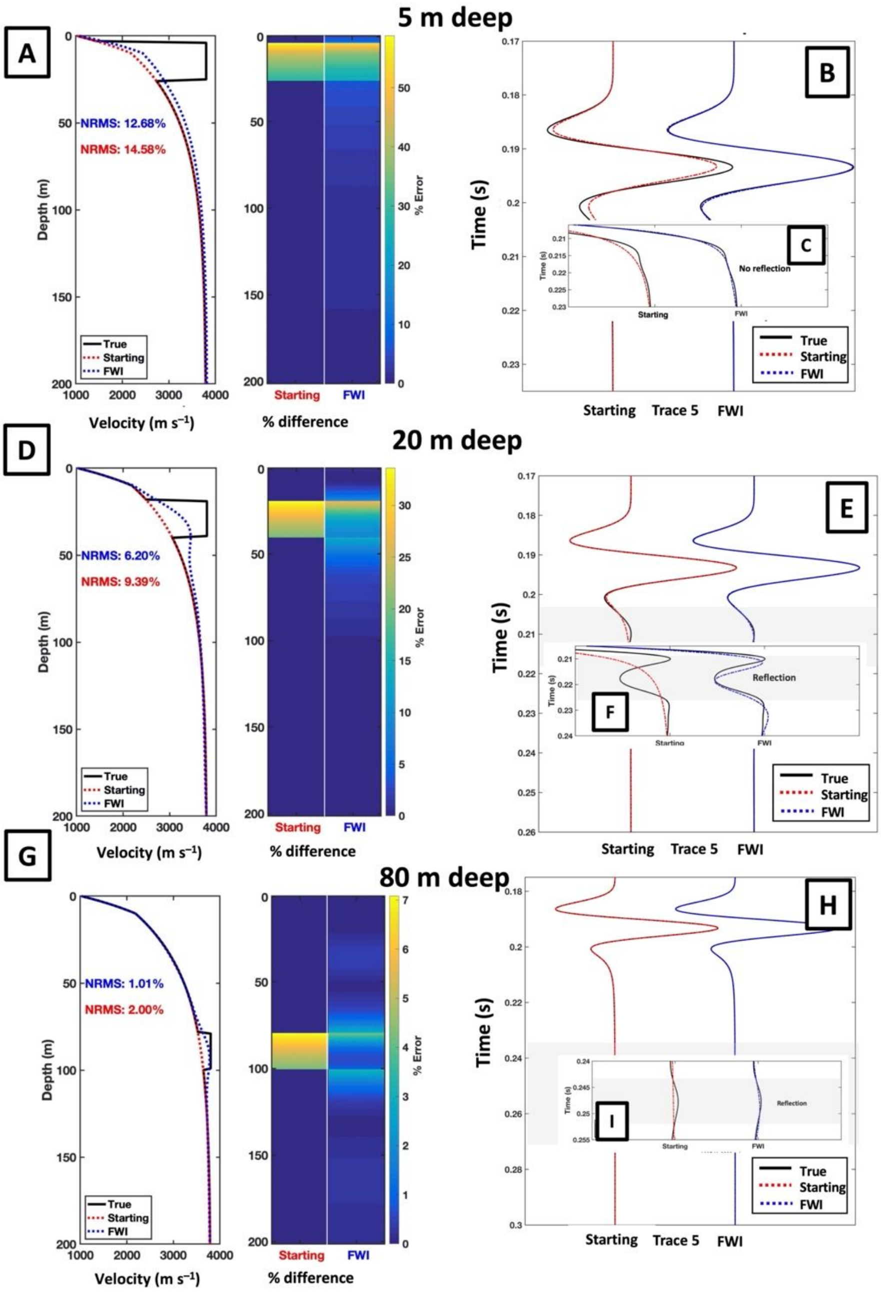

Figure 12: Velocity models for ice slabs at varying depths (left), the associated percentage error for every 1 m depth sample (right) and the NRMS error for the whole velocity pro le. (A) Ice slab is not detected. (D) Velocity inversion begins to be recovered. (G) Velocity inversion detectable and update is a clear divergence from background velocity trend. . As ice slabs are located deeper in the firn, the velocity anomaly caused by their presence within the background firn

compaction trend, is proportionally smaller.

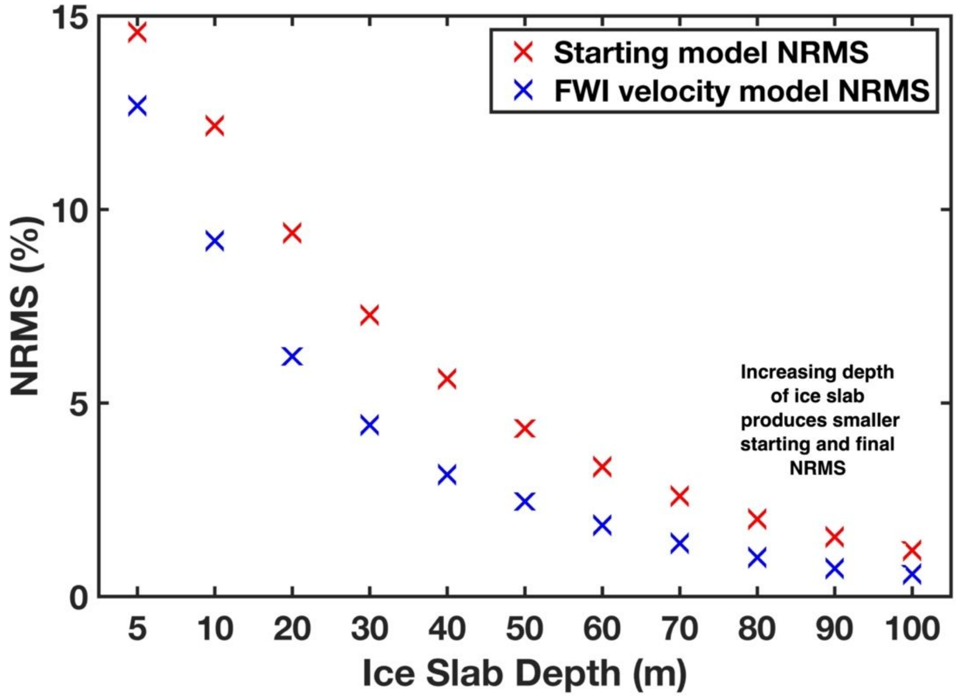

Figure 13: The reduction in NRMS achieved by FWI for models with increasing depth of the ice slab.

6. DISCUSSION

6.1 Advantages of FWI over conventional inversion approaches

The firn layer is important to understand as it can provide insight into the accumulation history of a glacier and should influence the design and interpretation of geophysical surveys that aim to explore basal glacier properties. We show that acoustic FWI can be used to improve reconstruction of the seismic structure of firn, compared to conventional traveltime tomography approaches. FWI can improve the recovery of the velocity structure of steady-state firn, leading to improved assessment of density and understanding of the accumulation regime. Furthermore, FWI yields accurate results even for poor starting models, provided that the deviation between the true and starting velocity models is small enough to avoid cycle skipping. We show that FWI can determine the depth and thickness of ice slabs located within the firn column, although the precise resolution and accuracy depends on the thickness and depth of the ice slab (improving with increasing depth and thickness).

Analysis of a range of synthetic firn structures, including steady- and non-steady state accumulation, show FWI can perform at least as well as HWI travel-time tomography approaches, but performs particularly well when ground-truth estimates of the shallowest seismic velocity structure are available. When FWI is used with the HWI velocity model as a starting model, the improvements of the velocity model accuracy produced by FWI are small (with a maximum NRMS reduction of 0.5% to the starting velocity model). An advantage of FWI, however, is that it can overcome errors in an HWI-derived starting model given its iterative model update. At the very least, the FWI output will be no worse than that initially derived from HWI .

Booth and others (2013) compared ground penetrating radar (GPR) with seismic refraction for reconstructing the thickness and density of glacier snow-cover. GPR was found to be more successful for accurately determining snow thickness, but seismic-derived velocities were more closely related to densities measured in a co-located snow pit. Although empirical relationships are still required to convert seismic velocity to density, FWI has shown that the velocity terms in such conversions can now be evaluated more reliably. Furthermore, with the extension of our acoustic FWI approach to an elastic inversion, it may be possible in the future to invert directly for firn density, thereby circumventing empirical approaches altogether.

6.2 Real-world applications of FWI methods

The presence of ice slabs influences meltwater drainage and runoff across glaciers and ice masses (MacFerrin and others, 2019). In the case of ice shelves, this decrease in permeability and increase in surface meltwater can lead to a reduction in ice shelf stability (Kuipers Munneke and others, 2014). This was observed on the Larsen B ice shelf, where firn compaction, meltwater ponding and hydrofracturing were strongly implicated in the ice shelf's rapid disintegration in 2002 (Scambos and others, 2004). FWI analysis of seismic data obtained over this region could have provided insight into the internal structure of the ice shelf prior to its collapse and motivates the application of FWI to existing ice shelves of concerning stability such as Larsen C Ice Shelf (LCIS).

Hubbard and others (2016) imaged a 40 m thick ice slab in a borehole located in Cabinet Inlet (in the upstream reaches of the northern sector of LCIS) and interpreted the ice as having formed from the accumulation of episodically refrozen surface meltwater ponds. Here the firn zone is 10^{o}C warmer and 170 kg m^{-3} denser than undisturbed firn in the surrounding area. Regional geophysical surveys suggested that the ice slab is at least sixteen kilometres across and several kilometres long. While GPR surveys (Booth and others, 2018) were able to constrain the layer's thickness and seismic velocity models (Kulessa and others, 2015) were consistent with pure ice, neither method could establish both the full depth extent and velocity anomaly of the slab. FWI methods show promise for applications such as this, particularly given that the thickness of the slab exceeds more than twice the wavelength of the seismic data presented in Kulessa and others (2015).

The next steps for FWI in glaciology are to apply these synthetic-based observations to real data. Notable requirements observed from the synthetic studies are the use of very near offset receivers to record the reflection from the ice combined with long offset to record the deep refractions. A form of ground truth in the very near offset will aid to prevent cycle skipping, and improve the likelihood of a successful FWI. The seismic source should also be as broadband as possible, featuring sufficiently low frequency to prevent cycle skipping while also including high frequencies to improve resolution.

7. CONCLUSION

It is important to be able to map firn structure and hydrology to understand process and to guide models of the stability of ice shelves, in particular the impact of impermeable ice slabs. Ice slabs can be detected and characterised by several geophysical methods, but FWI methods show potential for significant improvement over established methods. Using synthetic steady-state firn velocity profiles produced by the Herron and Langway densification model, we show FWI offers improved reconstructions over conventional approaches when the starting velocity model was a poor representation of the subsurface (as it commonly is). In non-steady-state cases featuring ice slabs, FWI improves the constraint of slab depth and thickness, which is currently impossible to do with established HWI approaches.

These synthetic analyses suggest that FWI should be considered in future seismic campaigns in glaciology, particularly over complex subsurface structure with minimal ground-truth control. The next steps for FWI in glaciology require the acquisition of FWI-compliant seismic data from real-world applications to validate our model approaches. Any location with ice slabs within the firn column would be appropriate, particularly at critical sites such as LCIS (e.g., for validation and the necessary shallow ground-truth constraint) makes it an attractive proposition for a test case.

ACKNOWLEDGEMENTS:

This research was funded by the Natural Environment Research Council of the UK, under Industrial CASE Studentship NE/P009429/1 with CASE funding from ION-GXT. Additional support was obtained from The International Association of Mathematical Geoscientists. Roger Clark and Emma Smith are thanked for their constructive discussion and support with this research and manuscript.

DATA AVAILABILITY:

Synthetic firn seismic velocity profiles are available to download from the figshare repository, https://doi.org/10.6084/m9.figshare.20765350.v1 (Pearce, 2022).

REFERENCES:

Aki K and Richards P (2002) Quantitative Seismology. University Science Books, 2 edition. ISBN 0935702962

Al-Yaqoobi AMA (2013) Full-waveform inversion to 3D seismic land data. Ph.D. thesis, Imperial College London

Aragao O and Sava P (2020) Elastic full-waveform inversion with probabilistic petrophysical model constraints. Geophysics, 85(2), R101-R111

Ashmore DW, Hubbard B, Luckman A, Kulessa B, Bevan S, Booth A, Munneke PK, O’leary M, Sevestre H and Holland PR (2017) Ice and firn heterogeneity within Larsen C Ice Shelf from borehole optical televiewing. Journal of Geophysical Research: Earth Surface, 122(5), 1139–1153

Babcock E and Bradford J (2014) Quantifying the basal conditions of a mountain glacier using a targeted full-waveform inversion: Bench Glacier, Alaska, USA. Journal of Glaciology, 60(224), 1221–1231

Bai J and Yingst D (2014) Simultaneous inversion of velocity and density in time-domain full waveform inversion. In SEG Technical Program Expanded Abstracts 2014, 922–927, Society of Exploration Geophysicists

Banwell A (2017) Ice-shelf stability questioned. Nature, 544(7650), 306-307

Ben-Menahem A and Singh S.J (2012) Seismic waves and sources. Springer Science & Business Media

Benson CS (1962) Stratigraphic studies in the snow and firn of the Greenland ice sheet. Technical report, Cold Regions Research and Engineering Lab HANOVER NH

Bevan S, Luckman A, Hubbard B, Kulessa B, Ashmore D, Kuipers Munneke P, O'Leary M, Booth A, Sevestre H and McGrath D (2017) Centuries of intense surface melt on Larsen C Ice Shelf. The Cryosphere, 11(6), 2743-2753

Booth AD, Clark RA, Kulessa B, Murray T, Carter J, Doyle S and Hubbard A (2012) Thin-layer effects in glaciological seismic amplitude-versus-angle (AVA) analysis: implications for characterising a subglacial till unit, Russell Glacier, West Greenland. The Cryosphere, 6(4), 909–922

Booth A, Mercer A, Clark R, Murray T, Jansson P and Axtell C (2013) A comparison of seismic and radar methods to establish the thickness and density of glacier snow cover. Annals of Glaciology, 54(64), 73-82

Booth A, Sevestre H, Kulessa B, Bevan S, Hubbard B, Luckman A, Kuipers Munneke, Buzzard S, Ashmore D, and O'Leary M (2018) Ground penetrating radar evidence of refrozen meltwater in the firn column of Larsen C Ice Shelf. In EGU General Assembly Conference Abstracts

Borisov D, Smith J, Tromp J, Miller R, Peterie S, Cudney H, Sloan S and Moran M (2017) Multi-component 3D Elastic Full Waveform Inversion Using Surface and Body Waves for Detecting Near Surface Anomalies. 79th EAGE Conference and Exhibition 2017

Bôcher M (1909) On the regions of convergence of power-series which represent two-dimensional harmonic functions. Transactions of the American Mathematical Society, 10(2), 271-278

Bradford J (2010) Simultaneous estimation of water saturation and porosity in the vadose zone by common parameterization of seismic P-wave and GPTr velocities. In AGU Fall Meeting Abstracts, volume 2010. pp. NS44A–03. 18

Brittan J, Bai J, Delome H, Wang C and Yingst D (2013) Full waveform inversion–the state of the art. First Break, 31(10), 75–81

Brisbourne A, Martin C, Smith A, Baird A, Kendall J, and Kingslake J (2019) Constraining recent ice flow history at Korff Ice Rise, West Antarctica, using radar and seismic measurements of ice fabric. Journal of Geophysical Research: Earth Surface, 124(1), 175–194

Chandler DM, Waller RI and Adam WG (2005) Basal ice motion and deformation at the ice-sheet margin, West Greenland. Annals of Glaciology, 42(1), 67–70

Church G, Bauder A, Grab M, Rabenstein L, Singh S and Maurer H (2019) Detecting and characterising an englacial conduit network within a temperate Swiss glacier using active seismic, ground penetrating radar and borehole analysis. Annals of Glaciology, 60(79), 193–205

Courant R, Friedrichs K, and Lewy H (1967) On the partial difference equations of mathematical physics. IBM journal of Research and Development, 11(2), pp. 215–234. 70

Culberg R, Schroeder D and Chu W (2021) Extreme melt season ice layers reduce firn permeability across Greenland. Nature communications, 12(1), 1-9

Dai YH and Yuan Y (1999) A nonlinear conjugate gradient method with a strong global convergence property. SIAM Journal on optimization, 10(1), 177–182

Diez A, Bromirski P, Gerstoft P, Stephen R, Anthony R, Aster R, Cai C, Nyblade A and Wiens D (2016) Ice shelf structure derived from dispersion curve analysis of ambient seismic noise, Ross Ice Shelf, Antarctica. Geophysical Journal International, 205(2), 785–795

Diez A, Eisen O, Hofstede C, Bohleber P and Polom U (2013) Joint interpretation of explosive and vibroseismic surveys on cold firn for the investigation of ice properties. Annals of Glaciology, 54(64), 201–210

Diez A, Eisen O, Weikusat I, Eichler J, Hofstede C, Bohleber P, Bohlen T, and Polom U (2014) Influence of ice crystal anisotropy on seismic velocity analysis. Annals of Glaciology, 55(67), pp. 97–106

Endres AL, Murray T, Booth AD and West LJ (2009). A new framework for estimating englacial water content and pore geometry using combined radar and seismic wave velocities. Geophysical Research Letters, 36(4)

Fomel S, Sava P, Vlad I, Liu Y and Bashkardin, V (2013) Madagascar: Open-source software project for multidimensional data analysis and reproducible computational experiments. Journal of Open Research Software

Gómez L and Pestana RC (2017) Full-waveform inversion using alternative objective functions in the presence of noise and uncertainties of source signature. In 15th International Congress of the Brazilian Geophysical Society & EXPOGEF, Rio de Janeiro, Brazil, 31 July-3 August 2017 (pp. 296-301). Brazilian Geophysical Society

Guasch L, Warner M, Nangoo T, Morgan J, Umpleby A, Stekl I and Shah N (2012) Elastic 3D full-waveform inversion. In 2012 SEG Annual Meeting. OnePetro

Herglotz G (1907) Über das Benndorfsche problem der Fortplanzungsgeschwindigkeit der Erdbebenstrahlen. Zeitschr für Geophys, 8, 145–147

Herron MM and Langway CC (1980) Firn densification: an empirical model. Journal of Glaciology, 25(93), pp. 373–385. ISSN 00221430.

Hollmann H, Treverrow A, Peters LE, Reading AM and Kulessa B (2021) Seismic observations of a complex firn structure across the Amery Ice Shelf, East Antarctica. Journal of Glaciology, 1–11

Hubbard B, Luckman A, Ashmore DW, Bevan S, Kulessa B, Munneke PK, Philippe M, Jansen D, Booth A, Sevestre H and others (2016) Massive subsurface ice formed by refreezing of iceshelf melt ponds. Nature communications, 7(1), 1–6

Jarvis EP, and King EC (1995) Seismic investigation of the Larsen Ice Shelf, Antarctica: in search of the Larsen Basin. Antarctic Science, 7(2), pp.181-190

Jones IF (2015) Estimating subsurface parameter fields for seismic migration: velocity model building. In Encyclopaedia of Exploration Geophysics, U1—-1, Society of Exploration Geophysicists

Jones IF (2019) Tutorial: The mechanics of waveform inversion. First Break, **37**, no.5, 31-43.

Killingbeck S, Schmerr N, Montgomery L, Booth A, Livermore P, Guandique J, Miller OL, Burdick S, Forster R, Koenig L and others (2020) Integrated borehole, radar, and seismic velocity analysis reveals dynamic spatial variations within a firn aquifer in southeast Greenland. Geophysical Research Letters, 47(18), e2020GL089335

King EC and Jarvis E (1991) Effectiveness of different shooting techniques in Antarctic firn. First Break, 9(6).

King EC and Jarvis EP (2007) Use of shear waves to measure Poisson's ratio in polar firn. Journal of Environmental and Engineering Geophysics, 12(1), pp. 15–21. 23, 26

Kinar N and Pomeroy J (2007) Determining snow water equivalent by acoustic sounding. Hydrological Processes: An International Journal, 21(19), pp. 2623– 2640.

Kirchner JF and Bentley CR (1979) Seismic short-refraction studies on the Ross Ice Shelf, Antarctica. Journal of Glaciology, 24(90), pp.313-319.

Kohnen H and Bentley CR (1973) Seismic refraction and reflection measurements at "Byrd" Station, Antarctica. Journal of glaciology, 12(64), pp. 101–111.

Kohnen H and others (1972) Uber die Beziehung zwischen seismischen Geschwindigkeiten und der Dichte in Firn und Eis. Geophysics, 38(5), pp. 925-935.

Kragh E and Christie P (2002) Seismic repeatability, normalized rms, and predictability: The leading edge, 21, pp. 640–647.

Kulessa B, Brisbourne A, Kuipers Munneke P, Bevan SL, Luckman AJ, Hubbard BP, Ashmore D, Holland P, Jansen D, King EC, O'Leary M and McGrath D (2015) Firn structure of Larsen C Ice Shelf, Antarctic Peninsula, from in-situ geophysical surveys. AGU Fall Meeting, 14-18 December 2015, San Francisco, USA, C21A-0708.

Lai CY, Kingslake J, Wearing MG, Chen PHC, Gentine P, Li H, Spergel JJ and van Wessem JM (2020) Vulnerability of Antarctica's ice shelves to meltwater-driven fracture. *Nature*, *584*(7822), pp.574-578.

Llorens MG, Griera A, Bons PD, Gomez-Rivas E, Weikusat I, Prior DJ, Kerch J and Lebensohn RA (2020) Seismic anisotropy of temper- ate ice in polar ice sheets. Journal of Geophysical Research: Earth Surface, 125(11), p. e2020JF005714.

Lutz F, Eccles J, Prior D and Hulbe C (2019) Constraining ice anisotropy and temperature from active source borehole seismology in the Ross Ice Shelf. In Geophysical Research Abstracts, volume 21.

Macchioli-Grande F, Zyserman F, Monachesi L, Jouniaux L and Rosas- Carbajal M (2020) Bayesian inversion of joint SH seismic and seismoelectric data to infer glacier system properties. Geophysical Prospecting, 68(5), pp. 1633–1656.

MacFerrin M, Machguth H, van As D, Charalampidis C, Stevens CM, Heilig A, Vandecrux B, Langen PL, Mottram R, Fettweis X and others (2019) Rapid expansion of Greenland's low permeability ice slabs. Nature, 573(7774), 403–407

Machguth H, MacFerrin M, van As D, Box JE, Charalampidis C, Colgan W, Fausto RS, Meijer HA, Mosley-Thompson E and van de Wal RS (2016) Greenland meltwater storage in firn limited by near-surface ice formation. Nature Climate Change, 6(4), pp.390-393.

Métivier L and Brossier R (2016) The SEISCOPE optimization toolbox: A large-scale nonlinear optimization library based on reverse communication: The SEISCOPE optimization toolbox. Geophysics, 81(2), F1–F15

Miller JZ, Culberg R, Long DG, Shuman, CA, Schroeder DM and Brodzik MJ (2022) An empirical algorithm to map perennial firn aquifers and ice slabs within the Greenland Ice Sheet using satellite L-band microwave radiometry. The Cryosphere, 16(1), pp.103-125.

Moczo P, Kristek J and Gális M (2014) The finite-difference modelling of earthquake motions: Waves and ruptures. Cambridge University Press

Moré JJ (1978) The Levenberg-Marquardt algorithm: implementation and theory. In Numerical analysis. Springer, 105–116

Mulder WA and Plessix RE (2004) A comparison between one-way and two-way wave-equation migration. Geophysics, 69(6), 1491– 1504

Mulder W and Plessix RE (2008) Exploring some issues in acoustic full waveform inversion. Geophysical Prospecting, 56(6), 827–841

Munneke PK, Ligtenberg SR, Van Den Broeke MR and Vaughan DG (2014) Firn air depletion as a precursor of Antarctic ice-shelf collapse. Journal of Glaciology, 60(220), 205–214

Nghiem SV and others (2012) The extreme melt across the Greenland ice sheet in 2012. Geophys. Res. Lett. 39, L20502

Nowack RL (1990) Tomography and the Herglotz-Wiechert inverse formulation. pure and applied geophysics, 133(2), 305–315

Paterson WSB (2016) The physics of glaciers. Elsevier, Pergamon, New York

Pearce E (2022) Synthetic firn seismic velocity profiles. figshare. Dataset. https://doi.org/10.6084/m9.figshare.20765350.v1

Peters L, Anandakrishnan S, Alley R and Voigt D (2012) Seismic attenuation in glacial ice: A proxy for englacial temperature. Journal of Geophysical Research: Earth Surface, 117(F2).

Plessix RE and Perez Solano CA (2015) Modified surface boundary conditions for elastic waveform inversion of low-frequency wide-angle active land seismic data. Geophysical Journal International, 201(3), pp. 1324–1334.

Pratt RG (1999) Seismic waveform inversion in the frequency domain, Part 1: Theory and verification in a physical scale model. Geophysics, 64(3), 888–901

Pratt RG, Gao F, Zelt C and Levander A (2002) A comparison of Ray-Based and Waveform Tomography-Implications for migration. In 64th EAGE Conference & Exhibition (pp. cp-5). European Association of Geoscientists & Engineers.

Rege R and Godio A (2011) Geophysical investigation for mechanical properties of a glacier. In Geophys. Res. Abstr, volume 13

Rintoul SR, Chown SL, DeConto RM, England MH, Fricker HA, Masson-Delmotte V, Naish TR, Siegert MJ and Xavier JC (2018) Choosing the future of Antarctica. Nature, 558(7709), 233–241

Riverman K, Alley R, Anandakrishnan S, Christianson K, Holschuh N, Medley B, Muto A and Peters L (2019) Enhanced firn densification in high-accumulation shear margins of the NE Greenland Ice Stream. Journal of Geophysical Research: Earth Surface, 124(2), pp. 365–382.

Scambos TA, Bohlander J, Shuman CA and Skvarca P (2004) Glacier acceleration and thinning after ice shelf collapse in the Larsen B embayment, Antarctica. Geophysical Research Letters, 31(18)

Schlegel R, Diez A, Lowe H, Mayer C, Lambrecht A, Freitag J, Miller H, Hofstede C and Eisen O (2019) Comparison of elastic moduli from seismic diving-wave and ice-core microstructure analysis in Antarctic polar firn. Annals of Glaciology, 60(79), pp. 220–230.
Schuster, G. T. (2017). Seismic inversion. Society of Exploration Geophysicists.

Shah N, Warner M, Nangoo T, Umpleby A, Stekl I, Morgan J and Guasch L (2012) Quality assured full-waveform inversion: Ensuring starting model adequacy. In SEG Technical Program Expanded Abstracts 2012, 1–5, Society of Exploration Geophysicists

Sirgue L (2006) The importance of low frequency and large offset in waveform inversion. In 68th EAGE Conference and Exhibition incorporating SPE EUROPEC 2006

Sirgue L, Barkved OI, Van Gestel JP, Askim OJ and Kommedal JH (2009) 3D waveform inversion on Valhall wide-azimuth OBC. In 71st EAGE Conference and Exhibition incorporating SPE EUROPEC 2009

Slichter LB (1932) The Theory of the Interpretation of Seismic Travel-Time Curves in Horizontal Structures. Physics, 3(6), 273– 295

Smith AM (2007) Subglacial bed properties from normal-incidence seismic reflection data. Journal of Environmental & Engineering Geophysics, 12(1), 3–13

Tarantola A (1988) Theoretical background for the inversion of seismic waveforms, including elasticity and attenuation. In Scattering and attenuations of seismic waves, part i (pp. 365-399). Birkhäuser, Basel.

Thiel E and Ostenso NA (1961) Seismic studies on Antarctic ice shelves. Geophysics, 26(6), 706–715

Van As D and others (2012) Large surface meltwater discharge from the Kangerlussuaq sector of the Greenland ice sheet during the record-warm year 2010 explained by detailed energy balance observations. Cryosphere 6, 199–209

Virieux J and Operto S (2009) An overview of full-waveform inversion in exploration geophysics. Geophysics, 74(6), WCC1– WCC26

Warner M, Ratcliffe A, Nangoo T, Morgan J, Umpleby A, Shah N, Vinje V, Štekl I, Guasch L, Win C and others (2013) Anisotropic 3D full-waveform inversion. Geophysics, 78(2), R59–R80

Widess MB (1973) How thin is a thin bed? Geophysics, 38(6), 1176– 1180

Wiechert E (1910) Bestimmung des Weges der Erdbebenwellen im Erdinneren, I. Theoretisches. Phys. Z., 11, 294–304

Williamson PR (1991) A guide to the limits of resolution imposed by scattering in ray tomography. Geophysics, 56(2), 202–207

Wuite J, Rott H, Hetzenecker M, Floricioiu D, De Rydt J, Gudmundsson GH, Nagler T and Kern M, (2015) Evolution of surface velocities and ice discharge of Larsen B outlet glaciers from 1995 to 2013. The Cryosphere, 9(3), pp.957-969.

Zhang JH and Yao ZX (2013) Optimized finite-difference operator for broadband seismic wave modeling. Geophysics, 78(1), pp. A13–A18.